12-2012

Laboratory Modeling of Critical Hydraulic Conditions for the Initiation of Piping

Mandie Swainston Fleshman

LABORATORY MODELING OF CRITICAL HYDRAULIC CONDITIONS FOR THE INITIATION OF PIPING

by

Mandie Swainston Fleshman

A thesis submitted in partial fulfillment
of the requirements for the degree

of

MASTER OF SCIENCE

in

Civil and Environmental Engineering

Approved:

_____	_____
Dr. John D. Rice Major Professor	Dr. James A. Bay Committee Member
_____	_____
Dr. Gilberto E. Urroz Committee Member	Dr. Mark R. McLellan Vice President in Research and Dean of School of Graduate Studies

UTAH STATE UNIVERSITY
Logan, Utah

2012

ABSTRACT

Laboratory Modeling of Critical Hydraulic Conditions

for the Initiation of Piping

by

Mandie Swainston Fleshman, Masters of Science

Utah State University, 2012

Major Professor: Dr. John D. Rice
Department: Civil and Environmental Engineering

Seepage-related erosion is one of the predominant mechanisms responsible for incidents and failures of dams and levees. Current geotechnical engineering practice consists of comparing expected exit gradients with the critical gradient of the soil at the seepage exit point. The critical gradient is generally considered as the ratio of soil buoyant unit weight and the unit weight of water, suggesting that the critical gradient only depends on the void ratio and specific gravity of the solids. However, in the field and in research, it has been observed that piping can initiate at average gradients much lower than unity due to concentrations in flow and non-vertical exit faces. Therefore, there is a need for deeper understanding of the granular scale mechanisms of the piping erosion process.

This thesis presents the results of a laboratory study to assess the effects that soil properties and exit face configurations have on the potential for initiation of piping

and the piping mechanisms. By using a laboratory device designed and constructed specifically for this study, the critical gradients needed to initiate piping in a variety of sandy soils were measured to assess the effects that parameters such as gradation, grain size, and grain shape have on the critical gradients. The tests are also used to observe the grain scale mechanisms of piping erosion initiation. The ultimate goal of the study is to develop an empirical, but mechanism-based, grain-scale model that can take into account the effects of converging flows, non-horizontal exit faces, and soil properties while assessing the potential for piping erosion to occur.

(92 Pages)

Mandie S. Fleshman

PUBLIC ABSTRACT
Laboratory Modeling of Critical Hydraulic Conditions
for the Initiation of Piping

The objective of this research is to provide fundamental understanding of the piping phenomenon. This will lead to practical solutions to the critical hydraulic conditions for piping that account for soil properties, direction of flow, stress condition and exit face conditions. In current geotechnical engineering practice, these factors are generally not considered. The critical hydraulic gradient is assumed to be only a function of the soil buoyant unit weight. In recent analyses, laboratory experiments, and field observations indicate that piping can be initiated at gradients much lower than the values predicted by the current practice. The current practice may be conservative under certain conditions.

Results of this research and the research to follow have the potential to transform the way that seepage-related erosion is analyzed in practice. The results of this thesis research is to provide the data to develop a mechanism-based approach that models the actual mechanisms of piping erosion and considers various soil parameters and exit face conditions that affect the initiation and propagation of piping erosion. This approach will be more accurate than the existing analysis methods and will have the flexibility to be applied to a vast array of seepage conditions. The improved analysis approach is expected to vastly improve the accuracy of the assessments of piping potential, increasing public safety and allowing for better utilization of funds available to renovate the aging Dams and levee systems across the U.S.

ACKNOWLEDGMENTS

I would like to thank Dr. Rice for providing this opportunity for me and for all of the guidance he has provided throughout the duration of this project. I would like to thank my committee, Dr. Rice, Dr. Bay, and Dr. Urroz, for the guidance they have provided though out the entire process. I would especially like to thank Dr. Bay and Ken Jewkes for all of their help in the lab, as well as Tammy Lee Jacobson and Rick Keizer, my undergraduate assistants.

I give special thanks to my husband, John Fleshman, for his patience and support throughout the research, as well as my parents and siblings who have also provided support and encouragement.

Mandie S. Fleshman

Contents

LIST OF TABLES

LIST OF FIGURES

CHAPT ER 1

INTRODUCTION

1.1 Piping Theory

Piping has caused failures in dams since the earliest dams were constructed around 2900 BC (Richards and Reddy, 2007). This seepage phenomenon continues to cause failures in dams and levees today. Seepage related erosion failure mechanism accounts for over 50 percent of dam and levee failures (Richards and Reddy, 2007). The current methods used to predict piping failure are based on theories that were developed in the 1940's (Terzaghi, 1943).

There are many different types of seepage failure mechanisms. The main three types are piping, concentrate leak, and heave. These seepage mechanisms have been studied by many people over the course of time.

Piping is internal erosion of the foundation or embankment soils caused by seepage forces. The erosion starts at the downstream toe and works backward toward the reservoir, forming pipes or channels under the dam or levee. Terzaghi (Terzaghi and Peck, 1948) presented a model of piping where soil particles are progressively dislodged from the soil matrix by the tractive forces produced by the seepage. These tractive forces are balanced by the shear resistance and weight of the soil particles. The erosive forces are greatest where the flow concentrates at an exit point. Once soil particles at this exit point are removed due to these forces, the magnitude of the erosive forces increases because the flow increases at this point. The forces that cause the removal of

grains in the soil are dependent on the hydraulic gradient through the soil as well as the state of stresses around the exit point (Richards and Reddy, 2007).

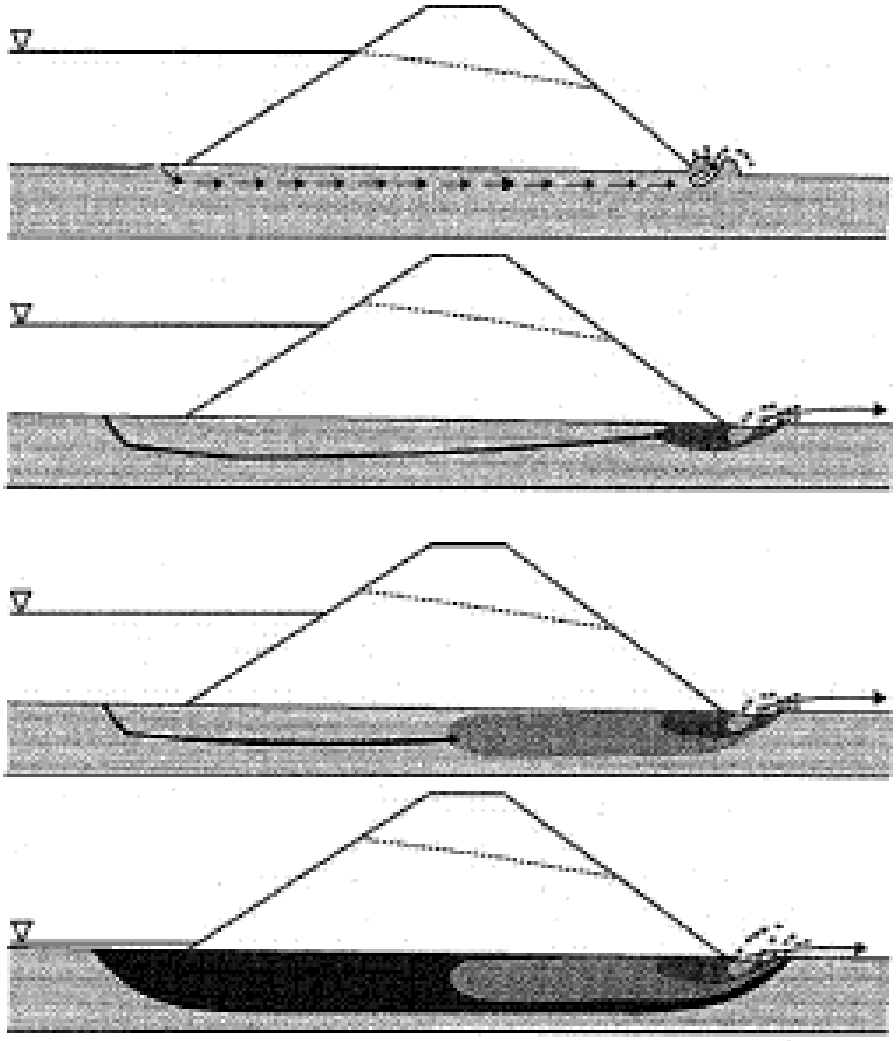

Figure 1. Piping failure (McCook, 2004).

Figure 1 shown above is a visual representation of how a piping failure progresses. As the reservoir is filled, seepage develops through a relatively permeable foundation. The foundation becomes saturated quickly. The water emerging at the toe of the dam causes particle movement and erosion of the foundation sands. This starts to form a boil. The sands in the foundation are then carried away and a tunnel begins to

develop in the foundation. If the embankment soils are able to form a bridge the tunnel or "pipe" will remain open. The backward erosion of the foundation continues to progress towards the upstream face. At this point the dam either collapses and overtops, or the reservoir is emptied through the underlying tunnel through the foundation.

Concentrated leak erosion is similar to piping. However, the concentrated leak erosion is due to flow along pre-existing openings in the embankment. These can be cracks in a cohesive soil or voids along a soil-structure contact. This type of seepage erosion is slightly different than piping in the forces that initiate the erosion. The tractive forces are along the length of the opening for concentrated leak erosion vs. piping where the forces are dependent on soil-to-soil contact. The hydraulic conductivity at a soil-structure boundary can be much higher than that of the surrounding soil. Therefore, fluid velocities can be more erosive for a given hydraulic gradient due to higher velocity flows (Richards and Reddy, 2007).

Heave occurs when a semi-permeable barrier overlays a pervious layer subject to relatively high fluid pressures. Terzaghi developed an equation for heave to assess heaving potential in sheet pile cofferdams. The pore water pressures in the pervious layer increases and a point may be reached where the uplift forces exceed the weight of the top layer of semi-permeable soils (Richards and Reddy, 2007), thus heaving the semi-permeable barrier.

In current geotechnical engineering practices seepage through soil is generally analyzed using Darcy's law:

$$Q = kiA$$ [Equation 1-1]

where *Q* is the flow, *K* is hydraulic conductivity, *i* is hydraulic gradient, and *A* is the cross-sectional area. Terzaghi developed the method that is most commonly used today to calculate the factor of safety against piping. He developed the theoretical equation:

$$i_{cr} = {\gamma'}/{\gamma_w}$$ [Equation 1-2]

where i_{cr} is critical gradient, γ' is soil buoyant unit weight, and γ_w is unit weight of water. In this equation the critical gradient only depends on the void ratio and the specific gravity of the soil. Terzaghi called the mechanism modeled by his relationship piping due to heave. However, this equation was developed for the heave mechanism, not the piping mechanism and thus a shortcoming in assessing piping potential. i_{cr} is often taken to be about unity for estimation purposes (Holtz and Kovacs, 1981). However, in past research and in field observations, piping has initiated at critical gradients much lower than unity.

Laboratory tests conducted by Skempton and Brogan (1994) showed that the critical gradient of sandy soils can be less than unity. Skempton and Brogan conducted tests on well graded, stable soils and poorly graded soils. The well graded soils varied in critical gradient from 0.7 to 1.0, depending on the direction of flow. The unstable soils varied more drastically. In the case of horizontal flow the critical gradient could be roughly 1/5 of the values predicted in Terzaghi's equation (Equation 1-2). With vertical flow, the critical gradient was found to be roughly 1/3 the value predicted in Terzaghi's equation (Skempton and Brogan, 1994). Skempton and Brogan's results differ from this research because they were modeling suffusion with unstable soils. Also an average

gradient across the entire soil sample was reported, rather than grain scale gradients causing the erosion. In the field average hydraulic gradients lower than 0.1 have been observed. The near failures of Herbert Hoover Dike (Davis, 2010) and A. V. Watkins Dam (Vroman, 2005) were two such cases. However, in both cases horizontal seepage was observed.

Skempton and Brogan (1994) theorized that the piping triggered at lower hydraulic gradients was due to lower effective stresses acting on the finer fraction of the soil which is supported by a coarser-grained skeleton. This phenomenon was called segregation piping. The lower global gradients measured across the entire soil sample would be an average of the local gradients of the entire soil sample. The low measured gradient during piping is likely the result of the concentration of flow between larger particles due to the larger grained fraction of the soil matrix and thus constrictions in the flow path of the seepage. If the local gradients between the large particles could be measured they would probably have much higher gradients. Schmertmann (2000) also concluded that "because of the local flow concentration to the pipe, the required high gradients can easily occur at a pipehead in a dam with global gradients in the normal range."

In this study hydraulic gradients at the formation of piping or sand boils, measured in the labratory research were higher than the past research has presented. This is due to the differences in the laboratory testing. The past research has always measured global hydraulic gradients, across a significantly larger soil sample than the small soil samples used in this research. The past research did not measure the local

hydraulic gradints at the seepage exit points that initiat the piping erosion. Also, in the past research there have been complex flow paths and geometries at the seepage exit points that made accurate measurements of hydraulic gradients difficult. This research measured the hydraulic gradients across a small soil sample as well as at points within the soil sample. In order to measure the hydraulic gradients closer to the microscopic grain size scale needed to really understand the piping mechanism.

The critical hydraulic gradient depends on many more factors than just the void ratio and the specific gravity of the solids. These contributing factors also include soil particle size, gradation, direction of flow, exit face inclination, and stress condition. In the current analysis methods, Equation 1-2 is still used to evaluate the critical gradient, which could be potentially unconservative.

Three stages of piping development were identified in the research: initial heave, boil formation, and total heave. Several different soils were tested in the research. The sands varied in grain size, gradation, grain shape, and specific gravity. The test results indicated the following: 1) angular soils showed greater piping resistance, 2) graded soils showed greater piping resistance, and 3) soils with higher specific gravity showed greater piping resistance. Hydraulic gradients measured in this labratory research at the formation of piping or sand boils, were higher than past research has presented. This is due to the differences in the laboratory testing and the measurement of local hydrauic gradients (microscopic scale) rather than global hydrauilc gradints (macroscopic scale).

1.2 Purpose of Research

The purpose of this research is to investigate the mechanisms of backward erosion piping by measuring gradients that cause piping at a grain size scale. A seepage test cell, developed at Utah State University, has been used to perform tests to measure the critical gradients of a variety of sandy soils. This was done to overcome the shortcomings of Equation 1-2. The results from these tests were used to provide insights into the relationships between soil properties and critical hydraulic conditions. The test results also will be used to validate and test a computer model, to be developed by Dr. Tong Qiu at Pennsylvania State University, that will model the mechanisms responsible for backward erosion (piping) and is expected to greatly improve the ability to assess the potential for the initiation and progression of backward erosion piping.

1.3 Report Organization

This thesis includes 6 chapters. Chapter 1 is an introduction to the purpose of the research. Chapter 2 presents an overview of the literature reviewed which relates to this study. Chapter 3 discuses the seepage test cell developed for the research that was conducted. The evolution of the design of the test cell is presented, as well as the functions of the various pieces of the apparatus. Chapter 4 provides a detailed explanation on the set-up procedure, how a test is conducted, and the data collection. Chapter 5 presents an analysis of results. Chapter 6 presents the conclusions.

CHAPTER 2

LITERATURE REVIEW

2.1 Introduction

A literary review of prior research relating to this project was performed. It is organized by the various topics related to this research.

2.2 Evolution of Piping Theory

One of the first advancements made in understanding piping was made by Bligh in 1913. Bligh studied many structures of his time that failed due to a piping related problem in the foundations of the structures. He developed a way to estimate the critical head for the structure in question. In his theory he recognized the relationship between the length of the seepage path and the loss of head. Bligh proposed that:

$$\frac{L}{H_{crit}} = E \qquad \text{[Equation 2-1]}$$

where *L* is the length of base of the levee perpendicular to the flow of water, and H_{crit} is the critical head. The value *E* is the safe ratio that depends on the type of material to be used. Bligh provided the value of *E* for four different types of soils given in Table 1. Bligh based his theory and values of *E* on empirical data collected from existing failures of structures due to seepage erosion.

Table 1. Bligh's thumb rules for obtaining L/Hcrit (=E) (Sellmeijer, 1988).

Type of Foundation Material	E
Riverbeds of light sandy sand	18
Fine Micaceous Sand	15
Coarse-grained Sand	12
Boulders or Gravel and Sand	5 to 9

The length of the seepage path which Bligh called the length of percolation is the shortest path between upstream and downstream of the structure. This simple relationship between seepage path length and the differential head across the structure could be used to assess the safety of an existing structure or in the design of a structure. Bligh developed his safe values of *E*, shown in Table 1, for the different types of soils that could be used for the foundation of a structure. The idea was to use the value of *E* and the differential head to calculate the required length of the seepage path. Bligh concluded that lengthening the toe apron of the structure would just increase the uplift pressures at the base and cause a failure. He discussed that placing vertical walls under the structure could be used to increase the seepage path, as well as extending the upstream apron (Bligh, 1910, 1913).

Lane (1934) improved upon Bligh's theory by accounting for vertical movement of flow lines and anisotropy. Lane developed his *weighted creep theory* from the analysis of dams all over the world. His conclusion was that horizontal seepage has less effect reducing uplift than vertical seepage. He suggested using a factor of 1/3 to be applied to horizontal seepage lengths when calculating the seepage lengths. Lane's empirical method took into account the erosion resistances of different types of soils. Lane empirically correlated the different piping resistances of soils by soil type and

incorporated this into his Weighted Creep Ratio analysis method (1934). Lane's weighted creep ratios are shown below in Table 2.

Table 2. Lane's Weighted Creep Ratio.

Material	Safe Weighted Creep Ratio (Lane 1934)
Very Fine Silt or Sand	8.5
Fine Sand	7
Medium Sand	6
Coarse Sand	5
Fine Gravel	4
Medium Gravel	3.5
Coarse Gravel, Including cobbles	3
Boulders with Some Cobbles and Gravel	2.5
Soft Clay	3
Medium Clay	2
Hard Clay	1.8
Very Hard Clay or Hardpan	1.6

Terzaghi developed the method that is most commonly used today to calculate the factor of safety against piping. He developed the theoretical equation

$$i_{cr} = {\gamma'}/{\gamma_w} \qquad \text{[Equation 1-2]}$$

that is based on the ratio of the effective weight of the soil and the uplift pressure on that soil. Terzaghi called the mechanism modeled by his relationship piping due to heave. He described this failures as "seepage pressure of the water that percolates upward through the soil beneath the toe becomes greater than the effective weight of the soil" (Terzaghi and Peck, 1948). He distinguished this process from failures initiated by subsurface erosion, which he described as "subsurface erosion that starts at springs near the downstream toe and proceeds upstream along the base of the structure or

some bedding plane" (Terzahi, 1948; Terzahi et al., 1996). This is a piping failure. Terzaghi claimed that the subsurface erosion process (piping) "defies a theoretical approach." Terzaghi's equation used with modern engineering analysis (such as Finite Element Method seepage analysis, FEM) is the standard for assessing the piping potential, despite that it was derived for a heave mechanism.

2.3 Laboratory Testing and Mathematical Models of Piping Theory

Khilar developed a piping model for clayey soils that predicts whether plugging or piping will occur. Khilar determined that the outcome strongly depends on the size distribution of the migrating particles relative to the pore size distribution of the soil which the particles are moving through. Large particle movements will lead to plugging and stop the backward piping erosion from progressing. Very small particles will wash through and proceed to form a pipe. For the intermediate particle sizes, the outcome depends on the concentration of the particles in the seepage flow and the rate of erosion of the particles from the pore walls (Khilar et al., 1985).

Sellmeijer and various co-investigators of Delft Hydraulics and Delft Geotechnics Laboratories (Delft) in Netherlands performed flume tests on clean, fine to medium-grained sands to model the seepage of water below a structure on a sandy foundation. The downstream side of the model was covered by a lid which modeled the impervious soil layer. The seepage water exited through a slot along the tip of the downstream portion of the flume. This was to model a ditch in an impervious layer. Tests were performed by slowly increasing the upstream hydraulic head and observing when and

how piping erosion initiated and progressed. Sand boils appeared at a certain stage of the test but as the sand transferred out of the boil, an equilibrium state was reached. As the hydraulic head was increased the boil would transfer more material and equalize again. This process would continue until the seepage flow reached a critical value which was associated with the progressive erosion. The seepage gradients increases and resulted in the failure of the sandy foundation (de Wit, et al., 1981; Sellmeijer, 1988).

Schmertmann (2000) correlated the uniformity coefficient of clean sands with the average gradient in flume tests. Flume tests at University of Florida (UF) were used to investigate piping. A flume that initiated piping along a sloped soil surface was used in the research and the tests were performed using a variety of clean sands. Using the results of the UF and Delft flume tests, Schmertmann showed that the average gradients across the flume required to cause piping erosion were strongly correlated to the uniformity coefficient of the sand.

Schmertmann also developed a procedure for calculating *the No-Filter Factor of Safety* against piping. This took into account simple geometric factors, the hydraulic conductivity, and the uniformity coefficient of the eroding soil. In addition to the unit weight of the soil, these tests indicated that the critical gradient in sand is a function of the grain size and uniformity of the sand (Schmertmann, 2000). However, due to the complex flow paths at the seepage exit points as a result of the non-uniform geometry of the seepage area, it is difficult to accurately measure hydraulic gradients and flow directions at the exit points. Therefore, the true critical gradient, as a fundamental soil property, could not be accurately assessed. This limits the usefulness of the research

results to applications having similar geometry and uniform sand throughout the profile. These tests have provided insight into some of the mechanisms associated with backward erosion piping; however, the results of these studies have not been incorporated into quantitative piping potential calculations used commonly in practice.

Tomlinson and Vaid (2000) performed tests to investigate the effects of grain size ratio between parent soil and a prospective filtering material, confining pressure, filter thickness, and seepage forces on the potential for erosion of soil to occur through the filter material. Tomlinson and Valid concluded that the grain size ratio is the most important parameter in determining if a soil-filter system will develop piping erosion. Confining pressure had a minor negative impact on the stability of the system. This was due to the collapse of arches in the soil with increases in stress. Tomlinson concluded that rapidly increasing the gradient prevented a proper filtration zone from forming and allowing piping to occur at smaller gradients.

Ojha et al. (2001) developed a theoretical model for critical gradient based on the porosity and hydraulic conductivity of the soils. The model coupled Darcy's Law and energy conservation. This was useful in explaining the dependence the critical head has on porosity. Piping seepage paths were idealized as pipe flows with the length of the base of the structure. This allowed Ojha et al. to use the energy conservation equation (Ojha et al., 2001). One limitation of the model is when a permeability relationship that depends only on the particle size is used in Darcy's law, which makes the model no longer useful. However, the model can be used to estimate the relative effect of porosity on the critical head.

Ojha et al. (2003) also developed a physically based model for the computation of the critical head. It provides a theoretical basis for Bligh's empirical rules. The critical head is dependent upon the length of the structure, soil properties, and fluid properties. Soils with a high porosity have lower values of length to the critical head ratios in comparison with the less pervious soils. This is also the case with large particles, allowing for higher permissible critical heads as opposed to finer particles (Ojha et al., 2003). This model imitates Bligh's empirical model, which is based on a large number of field studies.

CHAPTER 3

SEEPAGE TEST APPARATUS

3.1 Introduction

The testing apparatus used to conduct the experiments is designed to measure critical gradients in soil under vertical flow (horizontal exit face) conditions as well as various sloping exit face conditions. Although sloping exit face conditions were not studied in this research, they will be tested in the future. A schematic illustration of the apparatus is presented in Figure 2. In this apparatus, water flows perpendicular to the exit face through a uniform soil cross-section, thus avoiding the issues with determining the magnitude of the exit gradient due to the asymmetric convergence of seepage flow at the exit location as discussed in Chapter 2 with respect to the work by Schmertmann and Sellmeijer (Schmertmann, 2000; Sellmeijer, 1988; Sellmeijer and Konders, 1991).

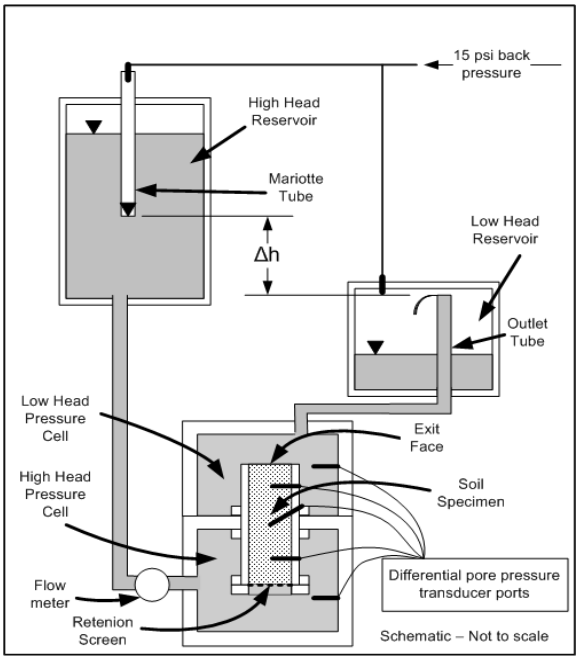

Figure 2. Schematic of testing apparatus.

The soil sample holder is a 5- inch long cylinder-shaped Plexiglas mold, 2- inch diameter with a retaining screen placed at the base to retain the soil and allow water to flow freely through the soil sample. The cylinder is sealed between two enclosed cells, the low-head pressure cell and the high-head pressure cell. The hydraulic heads of both cells are controlled by constant head tanks, one of which can be raised or lowered to change the differential head during a test. These are the high-head reservoir and the low-head reservoir which are attached to the high-head pressure cell and the low-head pressure cell, respectively. The head in the high-head reservoir is slowly raised via the Mariotte tube, until the erosion of the soil particles are observed at the exit face.

Three ports located at three elevations within the soil sample measure pore pressures at ¾ of an inch, 2- ¼ inches and 3- ¾ inches down from the top of the sample holder. Each pore pressure measurement is made by using a Validyne DP15-26 differential pressure transducer installed between the port and the low-head pressure cell. The total differential head across the sample is also measure using a differential pressure transducer. The magnetic-flux flow meter is installed between the high-head reservoir and the high-head pressure cell.

Campbell Scientific CR 1000 data logger is used to collect data every 0.1 seconds during a test. The data logger is connected to a computer so the data can be viewed in real time on the computer screen and saved for later analysis. Each test is videoed from the side and can be correlated to the data by the use of an electronic counter controlled by the data logger in the video field of view.

3.2 Design of Sample Holder

The soil sample holder is a 5-inch long by 2-in diameter cylinder-shaped Plexiglas mold. A screen placed at the base of the cylinder allows the retention of soil while allowing water to flow freely through the soil sample. There are three designs developed during this research as shown in Figure 3.

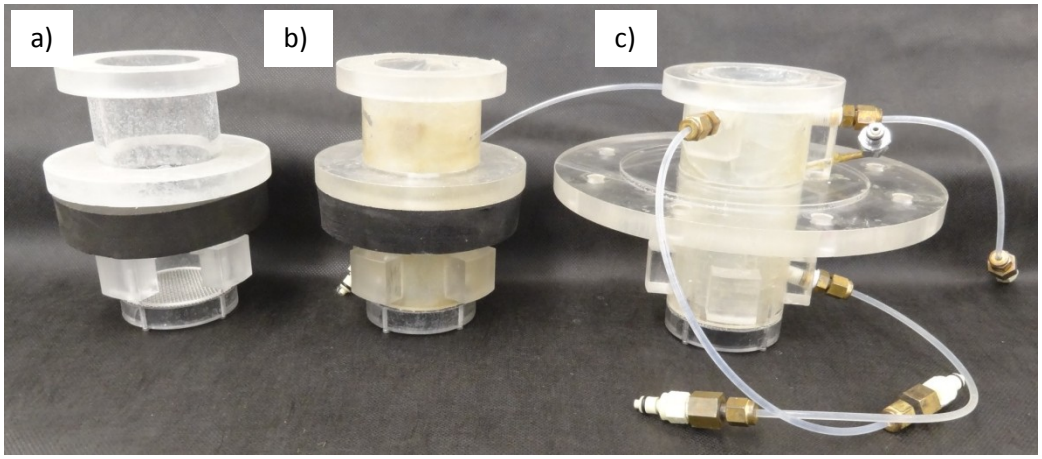

Figure 3. Soil sample holders: a) smooth-sided b) silicon-sided c) silicon-sided with instrumentation.

In the initial tests, the soil sample holder was a smooth-sided Plexiglas cylinder. The smooth sides allowed the soil to move freely along the inside surface of the sample holder due to the low friction between the smooth Plexiglas and the soil. This resulted in a heave of the entire soil mass during tests. The measured critical gradients conducted with the smooth sided cylinder were close to, if not exactly, the expected values calculated from Equation 1-2. The low friction angle did not model the resistance of soil-on-soil contacts that would be expected in a soil continuum. However, the purpose of the tests was to observe the initiation of a piping failure, not heave failure. To model the soil-to-soil contact, a silicon gel coating was placed along the inside

surface of the soil sample holder. This provided the friction needed to retain the soil from heaving and observe the grain-scale mechanisms of piping initiation. Sand grains also indented into silicon, thus reducing the potential for preferred seepage pathways along the side of the sampler.

The soil sample holder was again modified with additional instrumentation added to measure pore pressures within the soil sample. Three ports were located at three elevations within the sample. The pore pressure measurements occurred at ¾ of an inch, 2-¼ inches, and 3-¾ inches down from the top of the sample holder. For convenience these pore pressure ports were labeled PPA, PPB, and PPC, respectively, as can be seen in Figure 4. Each of the pore pressure measurements are made by using a differential pressure transducer installed between the port and the top reservoir. The total differential head between the reservoirs was also measured using a differential pressure transducer installed between the top and bottom reservoirs.

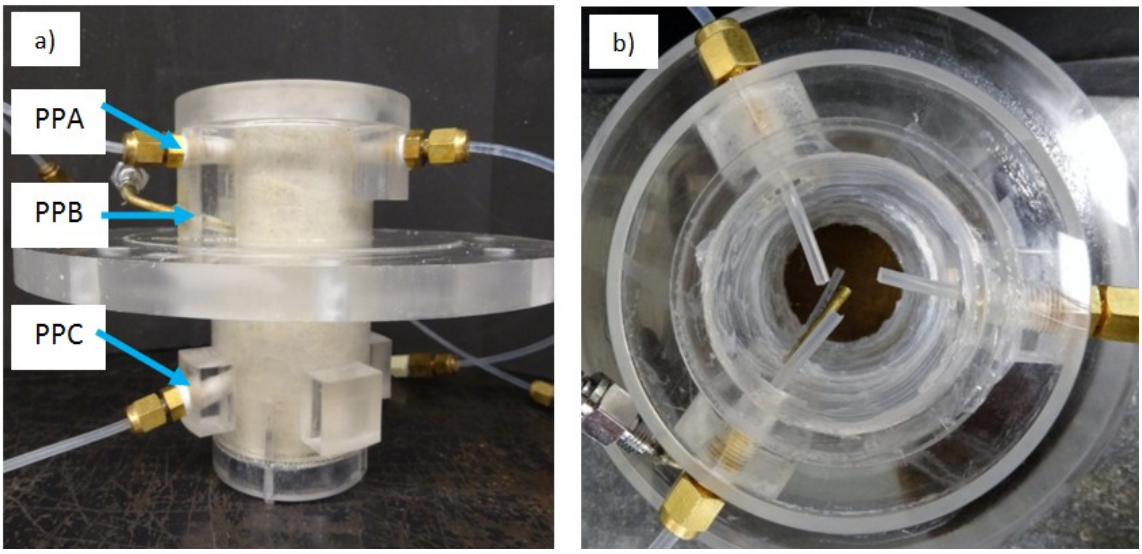

Figure 4. a) Location of pore pressure measurements and b) top view of soil sample holder.

3.3 Design of Differential Pressure Cells

The pressure cells are made of cylindrical sections of Plexiglas separated by a sheet of Plexiglas into two pressure cells, upper and lower pressure chamber as shown in Figure 5. Two 1-inch thick, 13-inch diameter cylindrical, Plexiglas plates are bolted to at the top and bottom of the pressure cells. These are sealed with o-rings and vacuum grease. Eight steel threaded rods are bolted to the top and bottom plates to seal the plates to the cylinders. Ports for vacuum and CO_2 lines are located near the top of the lower pressure cell and the top of the upper plate, respectively. These ports are quick connects that allow easy attachment and removal of the vacuum and CO_2. Three pore pressure measurement ports were installed through the top plate as well as one through the wall of the bottom pressure cell to allow the pore pressure measurements to be made in the sample. Two differential head measurement ports (also quick connects) are located close together through the sides of the top and bottom pressure cells.

Figure 5. Pressure cells.

The differential pressure cells have also had a few modifications from the original. The newest pressure cells are presented in Figure 5. The hole between the two cells was enlarged to allow for a larger diameter soil sample holder to be used. The Plexiglas ring around the smaller soil sample holder was enlarged and had holes drilled to allow the sample holder to be bolted into place. A rubber ring is compressed between the Plexiglas ring on the soil sample holder and the Plexiglas plate between the two pressure cells, to seal between the two pressure cells. The hydraulic heads of both pressure cells are controlled by constant head reservoirs.

3.4 Pressure Tanks

The constant head tanks have also been improved from the original design. The original design consisted of reservoirs open to atmospheric pressure that were supported on wooden platforms. One tank was at a constant elevation supported by the wood platform. The other tank was supported on four threaded steel rods and wing nuts to allow the platform to be raised and lowered to different elevations. This allowed a variable differential head between the two pressure cells during an experiment. However, because the reservoirs were open to the atmosphere, the total pressure (back pressure) that could be applied to the pressure cells was limited by the elevation of the reservoirs. A schematic figure of the original constant head tanks is shown below in Figure 6.

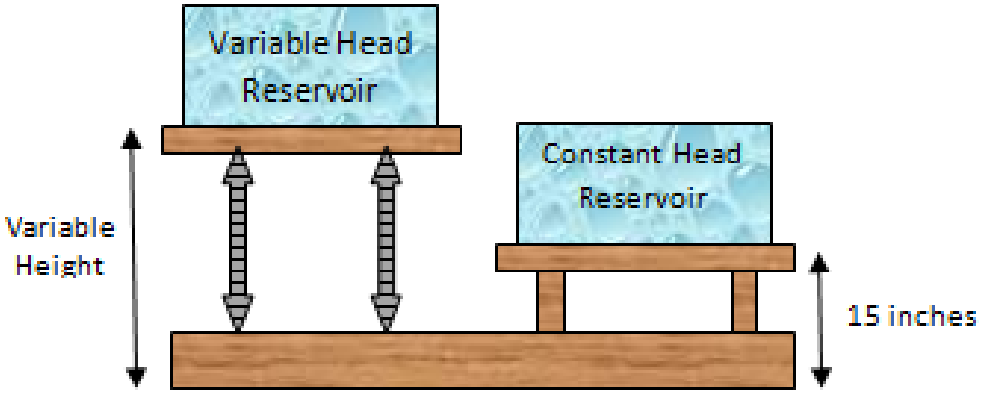

Figure 6. Schematic illustration of original constant head tanks.

To assist in the deairing of the samples, the new constant head reservoirs were designed. The reservoirs were modified to allow pressuring the system with 15 psi back pressure while maintaining the small differential head (about 0 to 0.8 psi). The head in the high-head reservoir attached to the high-head pressure cell can be adjusted to change the differential head across the sample. While the head in the low-head reservoir is attached to the low-head pressure cell and is set at a constant head. A schematic and picture of the new constant head reservoirs are shown in Figure 7.

In this system, the low-head reservoir is pressurized and the hydraulic head level is kept constant at the top of the outlet tube into the reservoir. The back pressure is applied to both the low-head reservoir and the high-head reservoir through the same pressure line, allowing both cells to be pressurized at the same rate. The back pressure to the high-head reservoir is linked to the Mariotte tube, Δh, is controlled by the difference in elevation between the top of the outlet tube in the low-head reservoir and the bottom of the Mariotte tube in the high-head reservoir. Because the back pressure

lines on the tanks are linked, the back pressure can be controlled independently of the differential pressure, significantly reducing the risk of overpressuring the sensors.

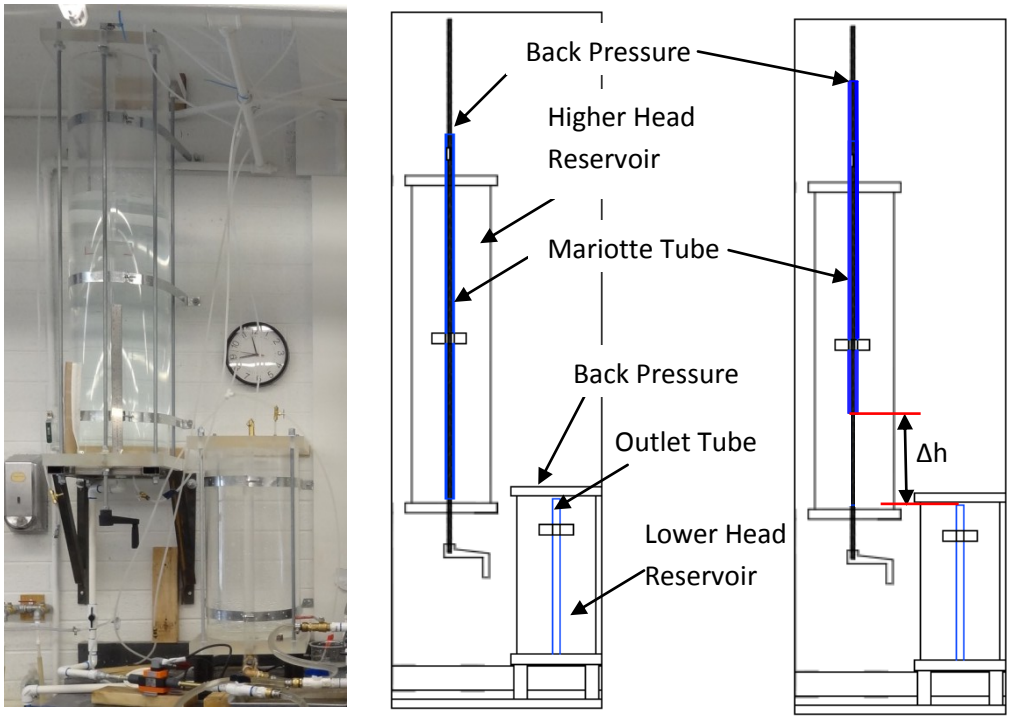

Figure 7. New constant head reservoirs.

3.5 Instrumentation

Instrumentation for the tests consists of the differential pore pressure transducers previously mentioned, and a magnetic-flux flow meter installed between the higher head reservoir and the high pressure cell. Data is collected using a Campbell Scientific CR 1000 data logger at 0.1 second intervals throughout the tests.

The four Validyne DP15-26 differential pressure transducers are connected to the pressure cells, soil sample, and the demodulator shown in Figures 8 and 9, respectively. One of the pressure transducers is connected between the top and bottom cells to measure the total differential head across the sample. The other three

transducers are connected between the lower pressure cell and one of the three pore pressure measurement ports in the soil sample. Electronic readings from the transducers are sent through the demodulator which converts the signal to a 0 to 20mAmp signal that can be read by the data logger. The demodulator has zero and span screws that are used to zero and calibrate the pressure transducer readings so that the data collected is displayed in inches of water. The pressure transducers were calibrated once and are checked regularly. The pressure transducers readings are zeroed at the beginning of each test.

Figure 8. Pressure transducers.

Figure 9. Demodulator.

The data logger used is a CR 1000 from Campbell Scientific as seen below in Figure 10. A program was written that controls how the data logger samples the flow meter and pressure transducers every tenth of a second and averages the readings over one second before storing them in a data file. The data logger is connected to a computer so that the data can be viewed and plotted in real time on the computer screen. Each test is videoed from the side. The timing of the video and data are correlated using an electronic counter displaying the passing seconds of the test. The electronic counter is attached to the outside of the lower pressure cell and is visible in the recorded video.

Figure 10. Data Logger CR 1000.

CHAPTER 4

TESTING PROCEDURE

4.1 Introduction

Detailed step by step instructions to set up and run the tests are included in Appendix A. A summary of this process is presented in this chapter.

4.2 Sample Preparation

The soil sample is prepared by using dry-raining and vibration technique. The sand is placed into the soil holder in small lifts (approximately ½ inch thick) and the soil container is tapped on the side to densify the sand by vibration. This resulted in consistent densities when duplicating the experiments. The soil holder is filled over capacity and struck off to produce a surface level with the top of the sample holder. This makes a soil sample that is five inches tall. The soil sample and the sample holder are then weighed and their weight is recorded. The weights allow the calculation of the buoyant soil unit weight, and are used to calculate the theoretical critical gradient using Equation 1-2.

The soil holder is then sealed between the pressure cells. The appropriate pore pressure connections need to be connected before the top plate of the pressure cells is placed. The bottom pore pressure port and tube needs to be connected before the soil holder is placed into the pressure cells. The pore pressure measurement tubes that go through the top plate need to be connected to the quick connections in the soil sample.

Once these connections are made, the top and bottom plates are bolted together to seal the pressure cells.

4.3 Saturation and Deairing

The valves are closed to completely seal off the pressure cells. To assist in the saturation, a vacuum is applied to the high-head pressure cell and a CO_2 line is attached to the low-head pressure cell. The CO_2 and vacuum are applied to the soil for 10 to 15 minutes, forcing CO_2 through the soil sample and replacing all of the air. CO_2 is more soluble in water than the gasses contained in atmospheric air and therefore speeds the process of saturation.

The vacuum is maintained until the soil sample is almost saturated with de-aired water. The pressure cells are filled with de-aired water from the low-head pressure cell. The de-aired water needs to be at a high enough flow to maintain a water column on top of the soil sample to avoid premature heave of the soil sample. The water will flow through the soil sample and begin to fill the high-head pressure cell. The vacuum can be removed at this point. The de-aired water valve is shut off after both pressure cells are filled.

4.4 Application of Differential Pressure

The differential pressure transducers are attached to lines leading to the ports in the sample holder and the readings are zeroed. With the pressure cells connected with a ½-inch bypass line to avoid buildup of differential pressure, the reservoirs are slowly

pressurized to 15 psi back pressure. The back pressure forces any remaining gas bubbles in the soil sample into solution and fully saturates the soil sample. It should be noted that some of the tests were run using the older constant head reservoirs that were open to atmospheric pressure. These did not have the ability to apply back pressure and therefore, saturation was achieved by allowing the sample to sit for several hours before testing.

4.5 Data Collection

The entire laboratory instrumentation set up can be seen in Figure 11. After pressurizing the cells, the data logger is turned on and the computer program, logger net, is opened on the connected computer. The data collection program is sent from the computer to the data logger. Data collection is started using a flag variable in the program that can be triggered from the computer terminal. This set up allows the output for the pressure transducers to be read in real-time on the computer screen, allowing the pressure transducers to be zeroed using the zeroing screws on the demodulator. After the pressure transducers are set and the zero readings are maintained, the data logger is prompted to collect data and is stopped while the zeroing data is deleted. This way, when each experiment is started, the start of the data will correspond to the electronic counter visible in the video.

With the test ready to start, the camera is set up so that the top of the soil sample is in view. The electronic counter is placed in the view of the camera but not blocking the view of the soil sample. To start the experiment, the camera is started, the

pulse counter is reset to zero, and the data logger is prompted to start collecting data. The counter visible in the video allows the recorded video and the test data to be correlated.

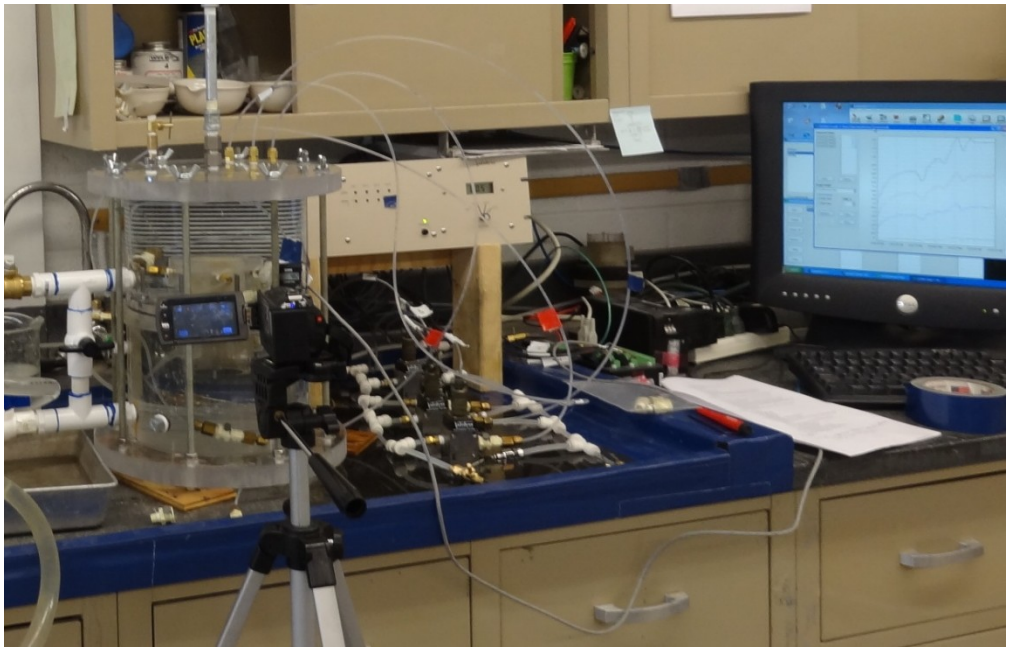

Figure 11. Test set up (minus the reservoirs).

4.6 Sample Failure

Each test is started with the bottom of the Mariotte tube and the tip of the outlet tube at the sample elevation (zero differential head across the sample). To increase the differential head across the soil sample, and thus increases the hydraulic gradient, the Mariotte tube is raised. A schematic of this process was shown in Figure 7 in Chapter 3. The Mariotte tube is slowly raised in one-inch increments until the sand starts to develop a failure mechanism. At this point the Mariotte tube is raised in half-inch lifts. After each incremental increase in differential hydraulic head, the differential hydraulic head is held constant for two to three minutes to give the soil time to react to

the increased differential head. The raising of the Mariotte tube is also paused when it looks like there is movement of the soil sample. This allows the soil sample time to react to the increasing hydraulic gradient and reach equilibrium with the seepage forces. The modes of failure observed in the test runs are discussed in Chapter 5.

After the soil sample has failed, the water valves are left open until the flow has leveled off. The water valves are then closed and the data logger is left on long enough to establish the zero reading at the end of the test. At this point the camera is turned off and the data is collected from the data logger. This data is saved to the computer and opened into an excel spreadsheet to be analyzed.

CHAPTER 5

TEST RESULTS

5.1 Introduction

Tests have been performed on a variety of sandy soils. Ottawa 20-30 and Graded sands conforming to ASTM C778-03 (well-rounded silica sands) were tested. In addition to these sands, samples of angular silica sand were prepared to the same gradations as the Ottawa 20-30 and graded sands. This was done to investigate the effect of grain shape on the critical gradient of the soils. Uniform, No. 16 sieve size angular quartz and uniform fine-grained, No. 100 sieve, garnet sand were prepared to investigate the effect of grain size on the critical gradient of the soils. The garnet sand has a much higher specific gravity than the quartz sands (3.87 verses 2.64 specific gravity for the quartz sands). In addition to these sands, samples with 2 percent by weight Kaolinite clay added to the fine-grained garnet sand were tested to investigate the effect of a small amount of cohesive soil would have on the critical gradient of the soil. A summary of the tests performed is presented in Table 3.

The soil samples have failed in several different ways: heaving, piping, or a combination of both. Piping is when a sand boil forms on the exit face and is caused when a preferential seepage pathway forms through the upper portion of the sample. The finer fraction of the soil gradation will be washed through the preferred pathway and deposited on the surface in a conical shape. Piping is pictured in garnet sand in Figure 12a.

Table 3. Results of critical gradient testing

Silicon Sided							
Soil Type			Average Gradient				
	Specific Gravity, G	Avg. Unit Weight	γ'/γ_w	First Visible Movement	First Sand Boil	Total Heave	Number of Tests
Angular # 16	2.64	93.33	0.93	1.24	-	2.16	5
Angular Sand 20-30	2.64	88.79	0.88	1.38	-	2.07	7
Angular Sand Graded	2.64	92.90	0.93	1.11	1.69	2.82	4
Garnet Sand (clean)	3.87	117.55	1.40	1.52	2.04	2.28	6
Garnet Sand w 2% Kaolinite Clay	3.87	115.65	1.38	0.80	1.95	2.26	2
Ottawa Sand 20-30	2.64	104.15	1.04	1.21	-	1.70	4
Ottawa Sand Graded	2.64	101.19	1.11	1.28	1.40	1.68	6
Fully Instrumented							
Soil Type			Average Gradient				
	Specific Gravity, G	Avg. Unit Weight	γ'/γ_w	First Visible Movement	First Sand Boil	Total Heave	Number of Tests
Angular Sand 20-30	2.64	92.29	0.92	1.48	1.75	2.72	3
Angular Sand Graded	2.64	96.41	0.96	1.39	2.03	2.95	7
Garnet Sand (clean)	3.87	128.17	1.52	1.73	1.76	2.89	4
Ottawa Sand 20-30	2.64	106.48	1.08	1.32	1.65	1.95	17
Ottawa Sand Graded	2.64	107.97	1.08	1.38	1.57	2.10	10

Heave occurs as the upper portion of the soil sample decrease in density resulting in the sample surface heaving upward and can be seen in Figure 12b. During the experiment, the soil column experiences a small heave at the top of the soil column and forms a bridge across the sample holder. When this happens, the increase in differential head is paused to allow the sample time to fully develop a failure mechanism before starting to increase the differential head again.

Three stages of failure were identified in the soils during testing: 1) first visible movement, 2) boil formation, and 3) total heave. The first visible movement is a slight movement of the exit face and could be described as slight movements of the uppermost sand grains as they reach a state of incipient motion. The soil particles on the surface of the soil sample start to move as the seepage forces exceed the resistive

forces (weight of particle, soil-on-soil contacts, etc). This movement often needs to be identified after the test by reviewing the recorded video to determine the start of the first movement.

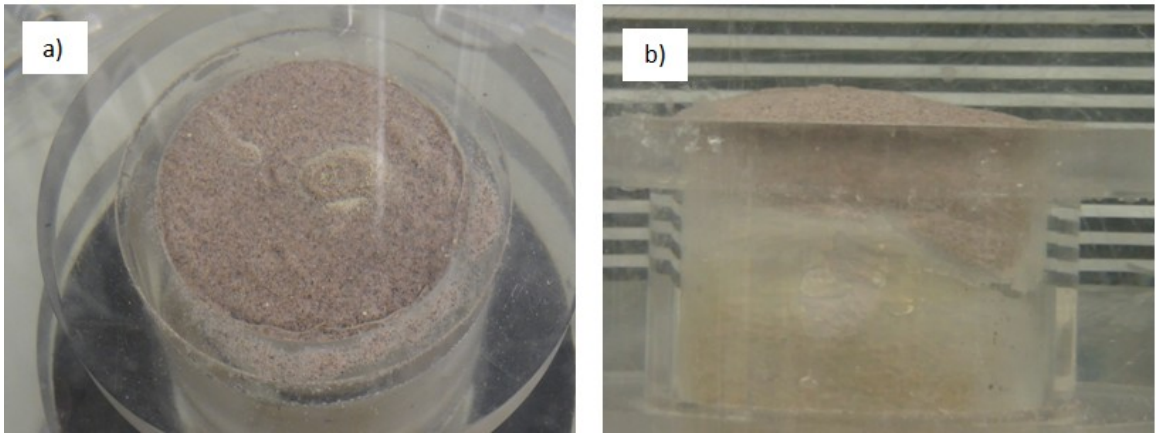

Figure 12. Sample failure mechanisms a) sand boil b) total heave.

As the differential head is increased, there is an increase in the viscous shear on the soil particles (seepage forces) that cause a loosening of the uppermost soil of the sample and what was called a heave movement. The soil loosens until equilibrium is reached. The equilibrium is achieved due to the reduction of the viscous shear on the soil particles in the loosened portion of the soil sample. The reduction in seepage forces is caused by the higher void ratio and thus higher permeability and lower seepage velocity in the loosened portion soil. As the differential head is increased the loosening of the top soil progresses downward until equilibrium is again reached.

The formation of a sand boil on the exit face is caused when a preferential seepage pathway forms through the upper portion of the sample. In graded soils, the finer fraction of the soil gradation is often washed through the preferred pathway and is deposited on the surface. In some cases the boil formation maybe the first detectible movement. In other cases, the third stage, total heave, occurs before a sand boil forms.

As the differential head is increased and there is an alignment of the interstitial voids, a sand boil forms. The differential pressure is relieved along the preferential flow path formed and equilibrium is established. This was also seen in Sellmeijer's research (Sellmeijer, 1988). This temporarily halts the downward progression of the loosening of soils, until the differential head is again increased.

The downward progression continues until the portion of the top soil that has heaved (loosened and increased void ratio) reaches an unstable configuration and begins to slough off to the sides of the sample holder. The sloughing removes some of the pressure of the overlaying soils and the third stage, total heave, occurs as the entire soil sample is heaved upward. A sand boil is presented in Figure 13a, and the sloughing off of the top soils that occurs just before total heave is presented in Figure 13b.

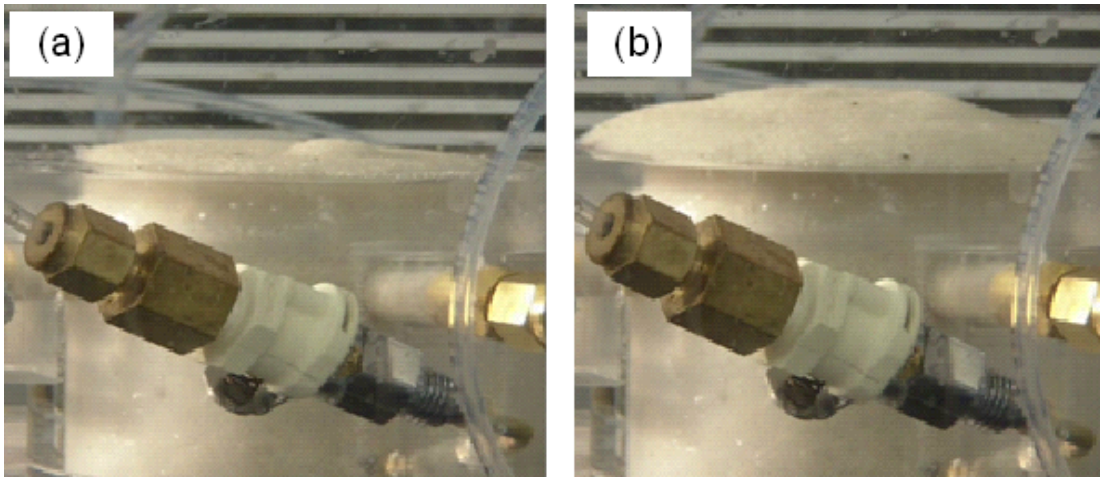

Figure 13. Photographs of (a) sand boil formation and (b) total have in a test on Graded Ottawa sand.

Using the electronic pulse counter in the video allowed the stages of failure to be correlated with the pore pressure data and therefore, the gradients at each stage. For each soil type tested, 1) the number of tests performed, 2) the average total gradients across the entire sample, and 3) the average gradients at which the three stages of

failure occurred are presented in Table 3. All of the data recorded for tests is presented in Appendix B. For comparison, the critical gradient calculated by Equation 1-2 ($i_{cr}= \gamma'/\gamma_w$) is also included in Table 3.

5.2 Types of Testing

Three types of sample holders that were discussed in Ch. 4, have been used for testing during the evolution of the test device: smooth-sided, silicon-sided, and fully instrumented. The fully instrumented sample holder is also coated with silicon, but has the three pore pressure measurement ports throughout the length of the holder. The results of gradients at the point when the sample reached total heave using the different sample holders on 20-30 Ottawa sand are presented in box plots shown in Figure 14 and results from Graded Ottawa sand are presented in box plots in Figure 15.

The tests performed using the smooth-sided holder resulted in a narrow band of critical gradient values slightly above a gradient of 1.0. These values are similar to what would be calculated using Equation 1-2. The narrow band is due to the heave mechanism being primarily a function of unit weigh, a parameter with little variation within a soil type. The critical gradients from the silicon-sided and fully instrumented holders are more widely distributed. The critical gradients are also higher than those tests performed with the smooth-sided holder. The increased variation in the silicon-sided holder is thought to due to random variation of soil structure within the samples that would result in local variations of bridging behavior and formation of preferred seepage pathways or boils, parameters that have a high level of variation but are not

important in the heave mechanism observed in the smooth-sided sampler. The higher critical gradients observed with the fully instrumented tests is attributed to a reinforcing affect the pore pressure ports have on the sample. Similar plots for the other soil types tested yielded similar results.

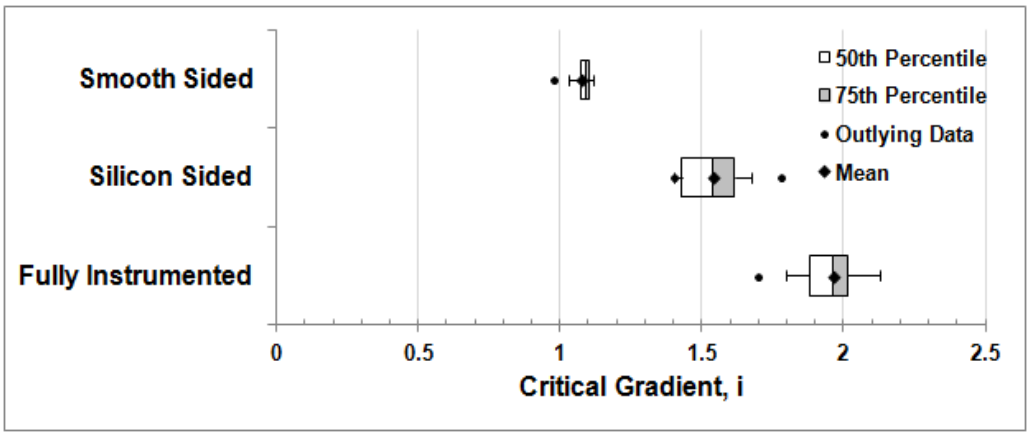

Figure 14. Sample holder results for total heave comparison 20-30 Ottawa sand.

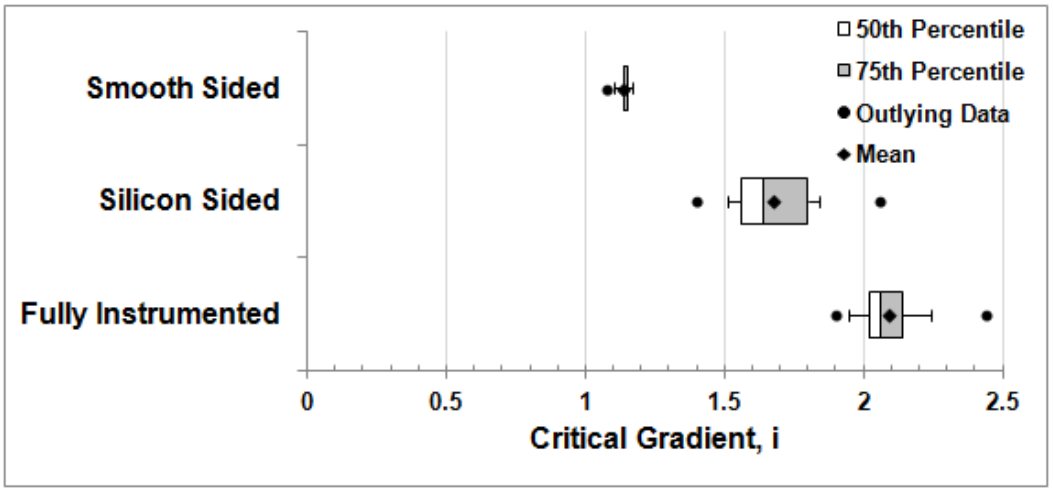

Figure 15. Sample holder results for total heave comparison Graded Ottawa sand.

All of the tests performed using the silicon-coated sample holder resulted in hydraulic gradients at total heave larger than the values calculated using Equation 1-2 for the respective soils. As previously mentioned, tests performed using the smooth-sided sample holder resulted in hydraulic gradients similar to or slightly higher than

those indicated by Equation 1-2. Though Equation 1-2 appears to be suitable for modeling the heave mechanism, the test results suggest that for the development of a piping failure there appear to be more factors affecting failure initiation than just the unit weight of the soil.

5.3 Comparison of Soils

Table 4 presents the soil properties that affect the critical gradient and how they affect the critical gradient. A discussion on the types of soils tested is presented below and how the properties presented in Table 4 affect the soil behavior.

Table 4. Soil types and critical gradient.

Factors Affecting Critical Gradient	**Soil Properties That Affect Critical Gradient**	**How Critical Gradient is Affected**
Interlocking	Grain Shape	Increases with angularity
	Gradation	Increases with wider gradation
Bridging	Grain Shape	Increases with angularity
	Gradation	Increases with wider gradation
Interstitial Void Shape	Grain Shape	Increases with angularity due to the irregularity of the particle shape
	Gradation	Increases with wider gradation due to the irregularity of the soil matrix
Interstitial Voids Size	Grain Shape	Decreases with angularity
	Gradation	Decreases with wider gradation
	Density	Increases with Density

A comparison of the gradients needed to cause full failure of the soils tested (total heave) is presented in Figure 16. The angular sands have higher critical gradients than their Ottawa (well-rounded) counterparts. This is believed to be due to the higher interlocking of soil particles resulting in more bridging of the soil in the sample holder. The angular 20-30 sand reached the points of the failure progression at lower gradients

than the graded angular sand. This was also true for the average gradients for the Ottawa 20-30 sand. The 20-30 sands reached total heave in the failure progression at lower gradients due to the higher uniformity of the interstitial void shape and size. There is less soil-on-soil contact and thus, less resistance to the viscous drag forces lifting the soil particles in the uniform soils. The soils with the wider gradation allowed for more variance in the interstitial voids shape and size as the smaller particles fill the voids between the larger particles. This provides more soil-on-soil contact to resist the viscous drag forces lifting the soil particles in the uniform soils.

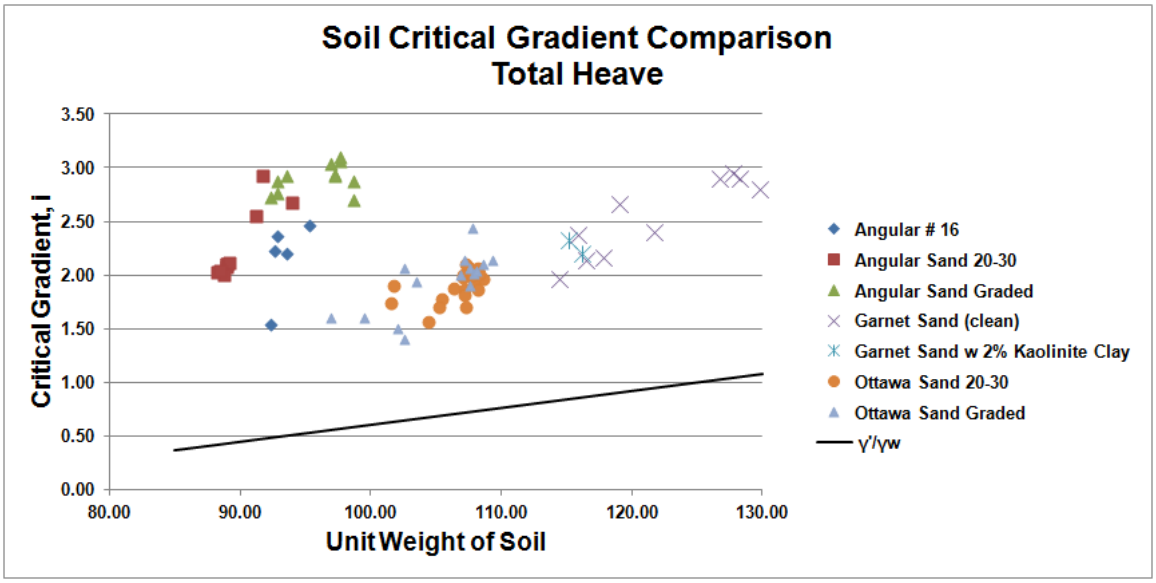

Figure 16. Comparison of measured critical gradient at final heave test results for various soils.

It was also observed that boils formed more often in the graded soils than the uniform soils (20-30 and Angular #16). The percentages of occurrences of piping for each soil type can be seen in Table 5. The observed higher gradients are thought to be due to two factors: 1) the gradation of the soil increases the bridging ability of the soil allowing higher gradients before heave and 2) the formation of boils in the graded soils

allows for dissipation of the pore pressures in the sample before total heave occurs. The Garnet sand also fails at higher gradients due mostly to the higher specific gravity although there may be some effect from the sub-angularity of the grains.

Table 5. Percentage of sand boils in soil types.

Material	**Percent of tests that involved formation of a pipe**
20-30 Angular Sand	30%
20-30 Ottawa Sand	76%
Garnet Sand	50%
Graded Angular Sand	92%
Graded Ottawa Sand	81%
No. 16 Angular Sand	0%

A comparison of gradients at the first visible movement of the soils tested is presented in Figure 17. This set of data has more variance than the total heave data. This could be due to random variation of soil structure within the samples that would result in local variations of bridging behavior, as well as human error in identifying the point of initial movement. The first movement is identified by reviewing the videos and detecting the first movement. This movement can be very slight and easy to miss.

The first movement data for the graded soils has a higher variance than the uniform soils. This is due to the increased potential for random variation of the interstitial voids in graded materials. Uniform soils have more uniform interstitial void shapes and better alignment of these voids. In graded sands the smaller particles settle between the larger particles creating a variety of interstitial void shapes, where the

uniform sands particles are all the same size and shape creating uniform interstitial voids.

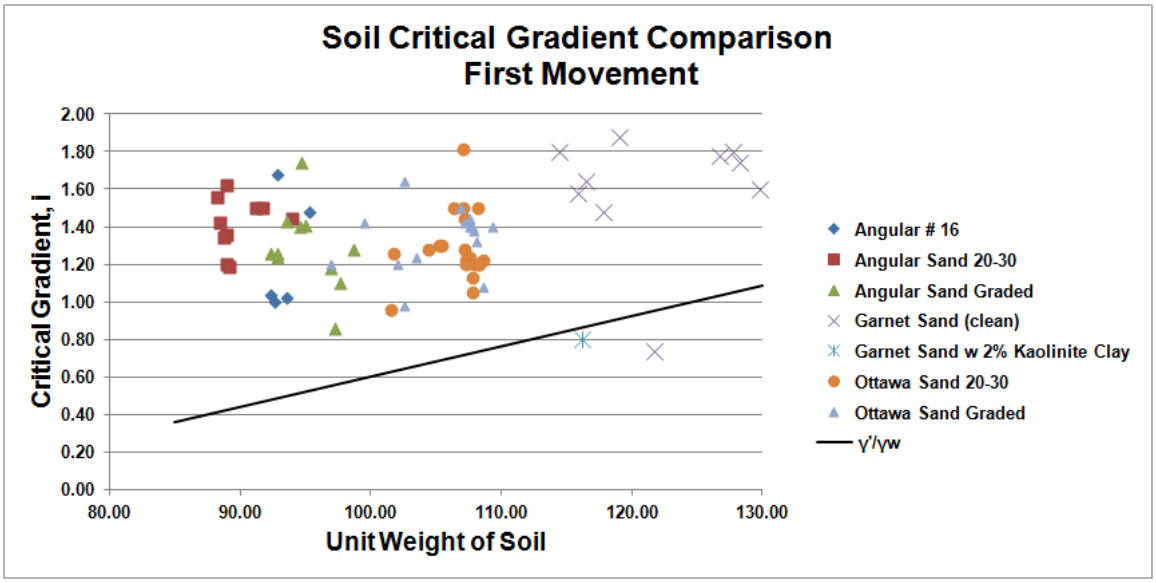

Figure 17. Comparison of measured critical gradient at first movement test results for various soils.

A comparison of the gradients at the occurrence of sand boils of the soils tested is presented in Figure 18. The uniform No. 16 sand did not form a pipe in any of the tests conducted on these soils. The other sands did not always form pipes, but data from the pipes that did form are shown in Figure 18 and the percentages of sand boil formation were presented previously in Table 5.

Angular sands show a higher gradient before a pipe forms and it can be concluded that angular sands have a higher resistance to piping. This could be due to the larger interlocking between soil particles in the angular sands than the smooth sided sands. The interlocking of soil particles causes the flow path in the interstitial voids to be longer and more sinusoidal. The interlocking of soil particles also resists upward seepage

forces due to higher bridging ability and thus the angular sand reached higher gradients before a pipe formed.

Graded soils also showed greater piping resistance. This could be due to larger interlocking between soil particles, more soil-on-soil contact, smaller seepage velocities between particles or less interstitial void alignment. The uniform soils show less resistance to piping than the graded soils. This could be due to the larger voids in between soil particles that allow more flow through the sample and thus a larger seepage velocity. This would displace the top soil particles of a uniform soil sooner than the top soil particles of a graded soil. Garnet sand has a higher specific gravity than the other sands used and displayed greater piping resistance. The Garnet sand has a higher specific gravity than the other sands and following with Teraghi's equation, it requires a higher gradient to initiate piping.

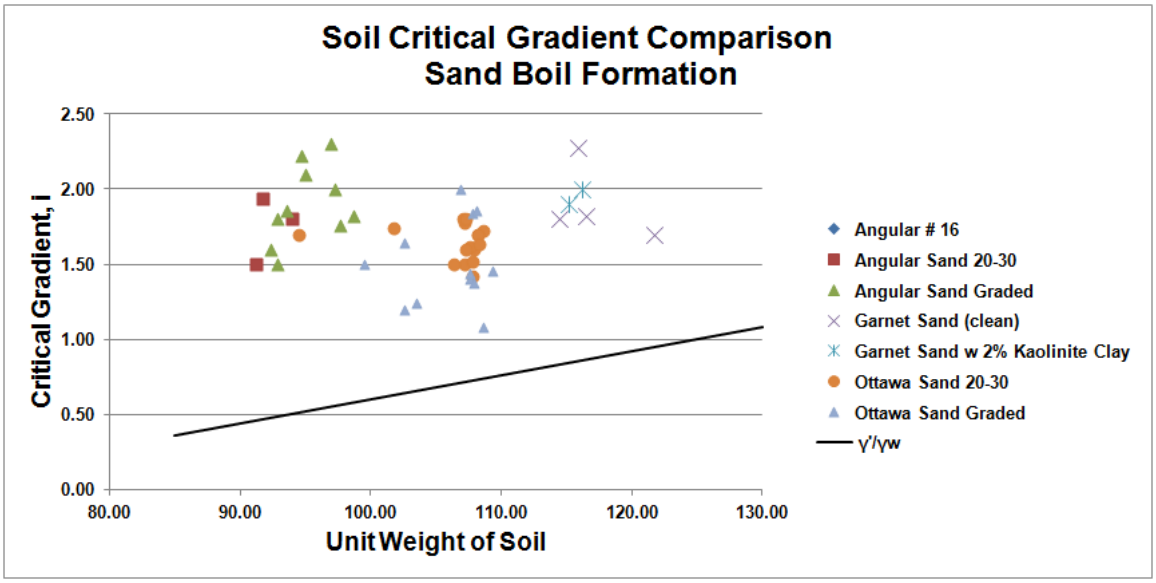

Figure 18. Comparison of measured critical gradient at the occurrence of sand boils for various soils.

5.4 Analysis of Data

For each test that was conducted, the data was analyzed by creating two different graphs. The first is a plot of the data collected that includes: 1) the total differential head, 2) differential head between each of the pore pressure ports and the lower pressure cell, and 3) the flow rate. An example of this graph is presented in Figure 19. To assist in the interpreting of the differential head data, the data from the pore pressure ports PPA, PPB, and PPC were normalized with respect to the total differential head and plotted. An example of the graph is presented in Figure 20.

The total differential head was normalized by dividing by itself to establish the base line of unity. The differential head measurements at PPA, PPB, and PPC were normalized by dividing by the expected differential head that would occur if the head drop was linear across the entire sample. The expected value was obtained by a linear fitting of the pore pressure data to the total differential head at low gradients as seen in Figure 21.

$$Normalized\ Differential\ Head = \frac{PP(A,B\ or\ C)}{m(total\ differetial\ head) + b} \qquad \text{[Equation 5-1]}$$

This corrects the total differential head to account for the head loss that occurs thorough the soil sample to the differential head measurements for PPA, PPB, and PPC. The normalized differential heads for PPA, PPB, and PPC should be equal to one until the soil sample has a change in permeability due to loosening of the soil or sand boil formation.

The linear fitting of the pore pressure data was calculated using only the linear portions of the data (i.e. from a total differential head of 1 inch to about 6 or 7 inches depending on the soil type). As seen in Figure 21, this linear fitting of the data was extrapolated to higher total differential heads and thus modeling the soils sample as if no loosening of soil occurred and therefore, no increase in permeability. Theoretically, the data could be normalized by dividing each differential head measurements at the pore pressure locations by the total differential head multiplied by the proportional distance from the bottom of the sample holder.

$$Normailzed\ Differential\ Head = \frac{PP(A,B,or\ C)}{Total\ diff.\ head*\left(1-\Delta x_{from\ bottom\ of\ soil\ sample}\right)} \quad \text{[Equation 5-2]}$$

This would correct the differential head measurement for the head loss that occurs through the soil sample. However, a linearization of the pore pressure measurements (PPA, PPB, and PPC) to the total differential head was required due to the slight differences in the linear calibration of the pressure transducers.

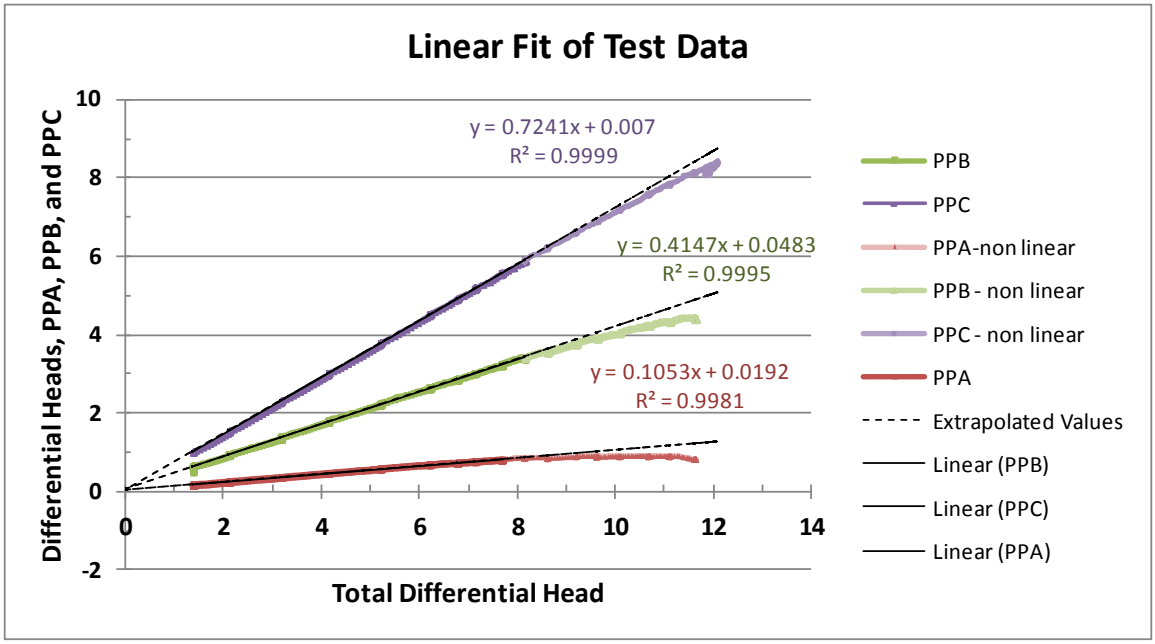

Figure 19. Linear fit of pore pressure measurements to total differential head.

Theoretically, all of the data should then equal one if there is no change in permeability during the duration of the test. However, as can be seen in the Figure 20, the differential head measurements at PPA, PPB, and PPC deviate from unity due to the change in the permeability of the soil as the soil loosens and due to the formation of sand boils. As each stage of the failure progression is reached the normalized test data can be seen deviating farther and farther from unity until total failure is reached and the soil sample heaves out of the soil sample holder.

After plotting the data as in Figures 19 and 20, the video of each test was reviewed and the failure progression was documented as follows: 1) the number of seconds passed, displayed on the electronic pulse counter, at each notable point in the failure progression was recorded and 2) the data for each differential head at that time was recorded. On both graphs of the test data, the stages of the failure progression were plotted. The various dashed and dotted vertical lines on the plots in Figures 19 and 20 represent the times at which the various stages of failure progression occurred.

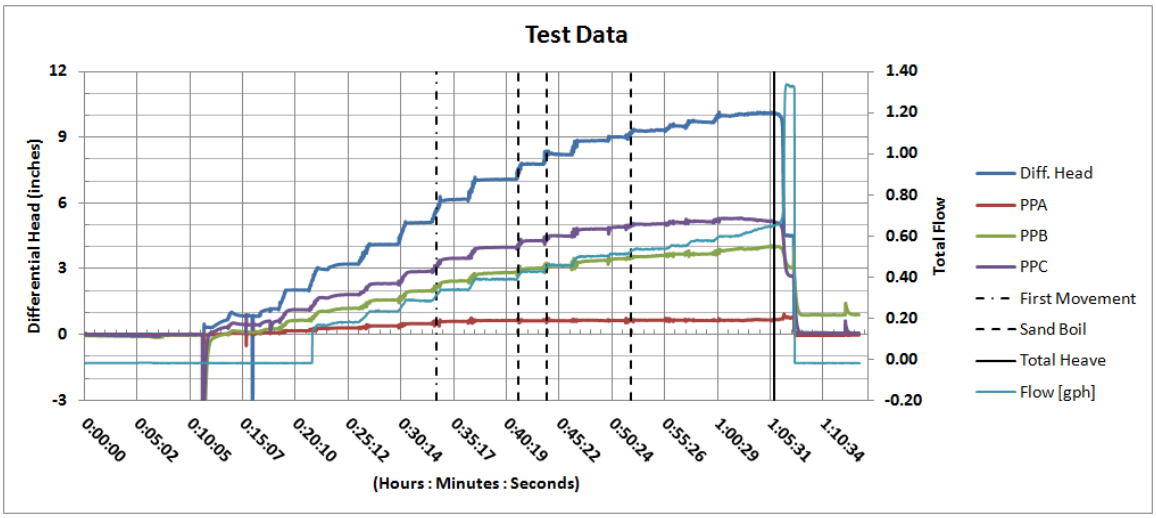

Figure 20. Test data for a 20-30 Ottawa sand (6/7/2012).

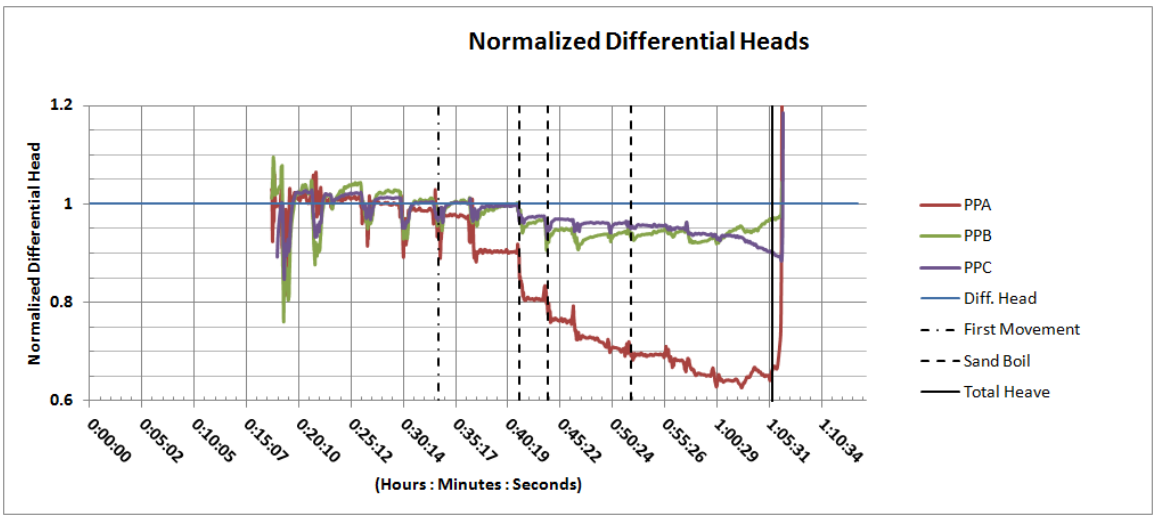

Figure 21. Normalized test data for a 20-30 Ottawa sand (6/7/2012).

5.5 Observed Progression of Failure Mechanisms

Evidence of the failure progression described in 5.1 can be seen in the instrumentation data presented in Figures 22 and 21. For this test on Graded Ottawa sand, the normalized data hovers around a value of 1.0 until the initial heave phase occurs. This occurred at a differential head of about 6 inches. The pore pressure ports begin to deviate below a normalized value of 1.0 and the deviation is most pronounced in PPA. The deviation is believed to be due to loosening of the surface soil (i.e. an increase in void ratio) which causes a decrease in flow resistance (increased hydraulic conductivity). With the flow resistance lowered in the upper portion of the sample, the head drop is concentrated in the lower portions. Therefore, the head drops across the upper portions of the sample are proportionally less than the overall differential pressure.

The continuation of the heave and associated downward progression of the loosened zone is reflected in the larger deviations of PPB and PPC toward the end of the

test. Each of the sand boils are accompanied by a drop in PPA, some larger than others. The first sand boil occurred at a differential head of close to 10 inches, at this point a large drop occurred in the normalized PPA plot. The second sand boil caused a small drop in normalized PPA, relieving more pressure built up in the top portion of the sample. The sand boils plugged and stopped flowing at about 26.5 minutes into the test; this was accompanied by an increase in the normalized differential head of PPA. The third sand boil to develop occurred and again relieved built up pressure in the top portion of the sample and an accompanying drop can be seen in Figure 23.

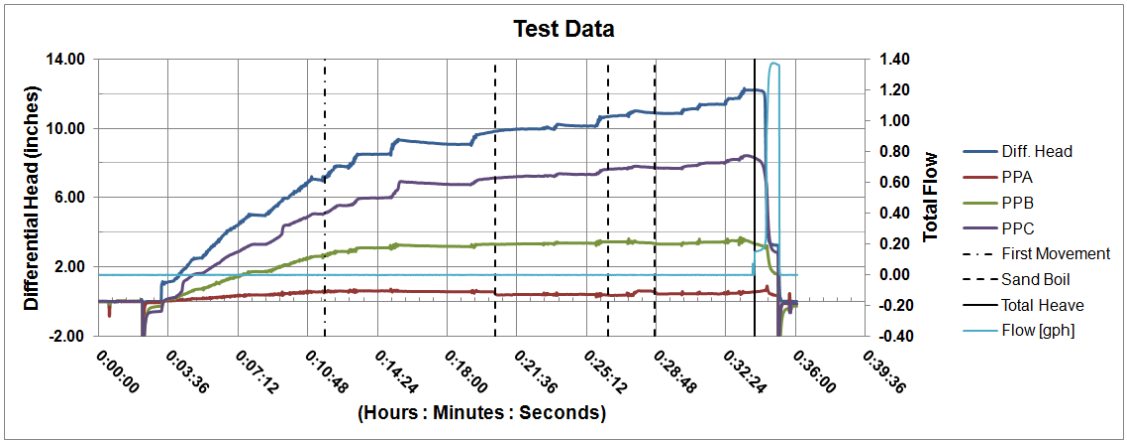

Figure 22. Test data for Graded Ottawa sand (4/12/2012).

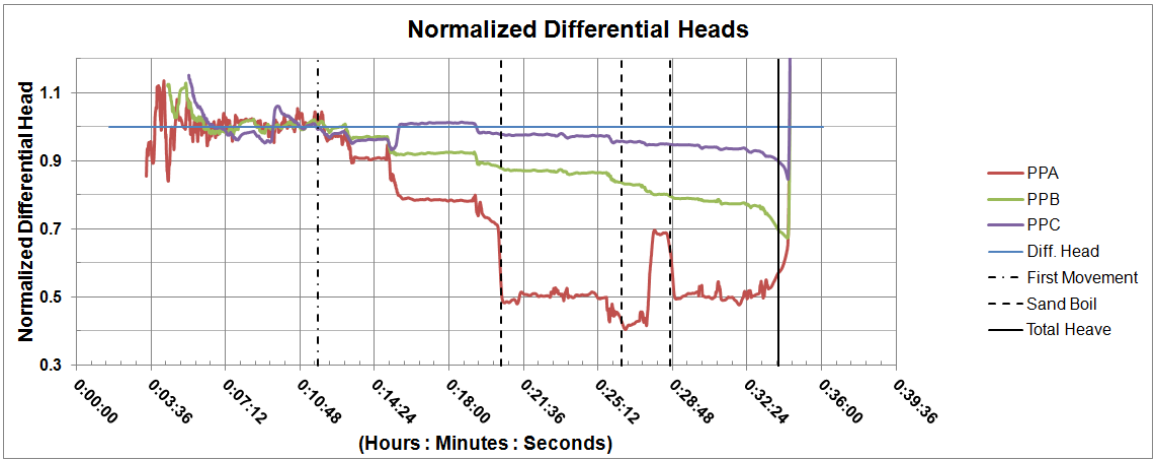

Figure 23. Normalized test data for Graded Ottawa sand (4/12/2012).

Evidence of the failure progression described in Chapter 5 can also be seen in the instrumentation data presented in Figures 24 and 25. For this test on 20-30 Ottawa sand, the normalized data hovers around a value of 1.0 until the initial heave phase occurs. This occurred at a differential head of about 6 inches and about 21 minutes into the test. The normalized differential head at PPA begins to deviate below a value of 1.0. The heaving of the soil continues and associated downward progression of the loosened zone is reflected in the deviations of PPB and PPC.

The first sand boil occurs between 8 and 8.5 inches of head at almost 29 minutes into the test. There is an associated drop in normalized differential head in PPA and PPB. The next sand boil occurred after just after the initial sand boil plugged. There was a small increase of the normalized heads in all three pore pressure measurements just before the associated drop in the normalized heads due to the sand boil formation. The third sand boil had a larger effect on PPB and PPC suggesting the progression of the pipe down to at least 3- ¾ inch from the top of the soil.

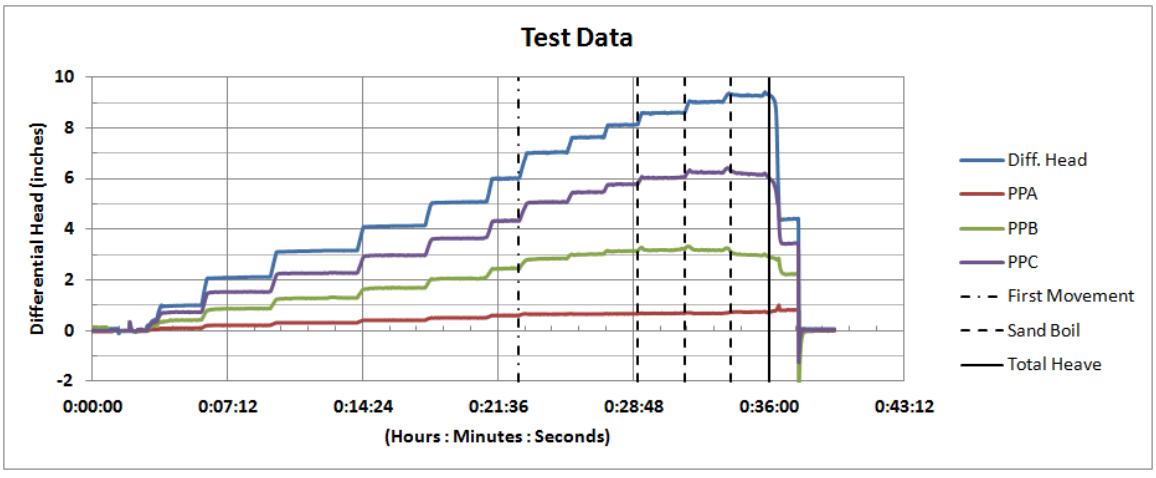

Figure 24. Test data for 20-30 Ottawa sand (6/21/2012).

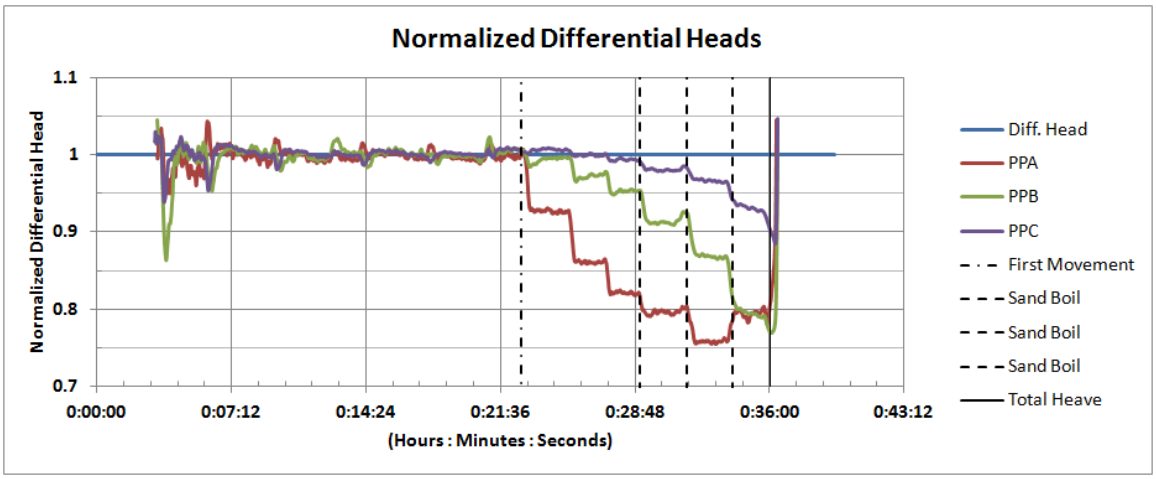

Figure 25. Normalized test data for 20-30 Ottawa sand (6/21/2012).

In the test on 20-30 Ottawa sand, shown in Figures 25 and 26, the normalized data hovers around a value of 1.0 until the initial heave phase occurs. This occurred at a differential head of about 7 inches and about 25 minutes into the test. The normalized data for PPA begins to deviate below a value of 1.0. The heaving of the soil continues and associated downward progression of the loosened zone is reflected in the deviations of PPB and PPC.

The first sand boil occurs between 8 and 8.5 inches of head at almost 30 minutes into the test. The second sand boil follows in quick succession. Both of these sand boils were accompanied by a drop in the normalized data for PPA, while only the first sand boil causes a drop in PPB. This occurred when the sample had a small heave movement and continued heaving until failure. The downward progression of the loosened zone can be seen near the end of the test, 48 minutes in to the test, both normalized and original data for PPB and PPC start dropping until the total heave is reached. When the small movement occurred it plugged the sand boils and the normalized data in PPA reflects this by slightly increasing until total heave occurred.

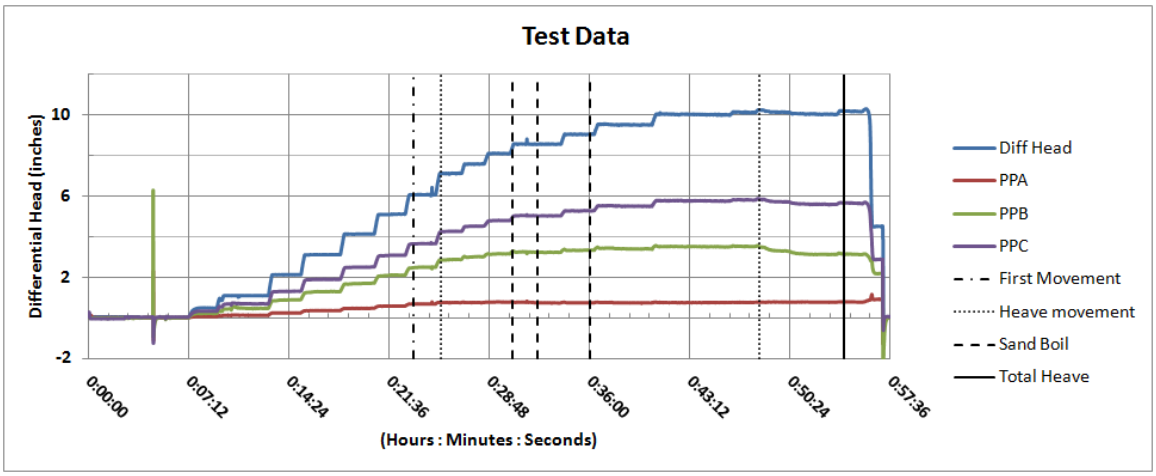

Figure 26. Test data for 20-30 Ottawa sand (6/19/2012).

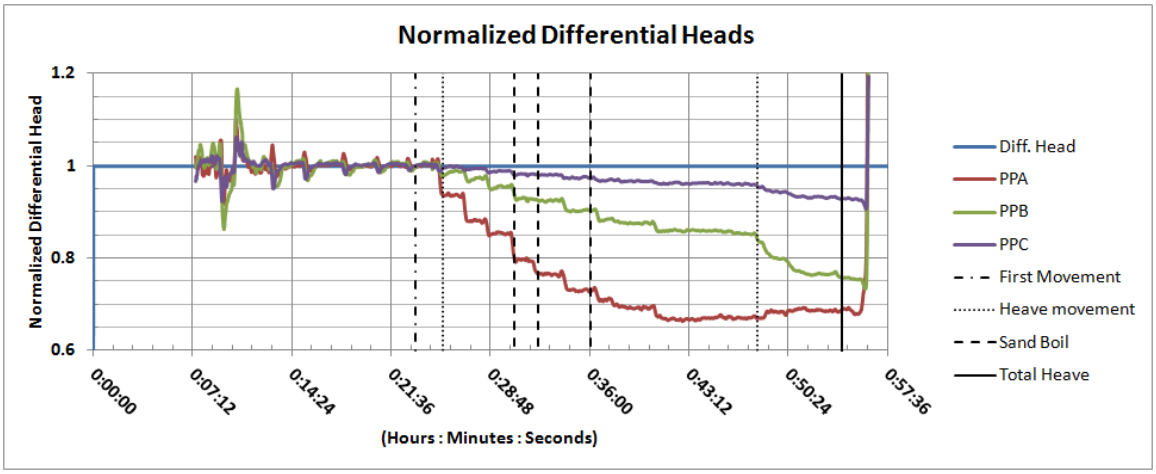

Figure 27. Normalized test data for 20-30 Ottawa sand (6/19/2012).

In the test on 20-30 Ottawa sand, shown in Figures 28 and 29, the normalized data hovers around a value of 1.0 until the first visible movement and the start of the heave phase. This occurred at a differential head of about 6 inches and about 19 minutes into the test. The normalized data for PPA begins to deviate below a value of 1.0. This initial movement is nearly imperceptible on the video and there is only a small drop in PPA. However, at the next heave movement at a total differential head of 7 inches, the heave movement was larger in addition to the associated drop in the normalized data for PPA.

It is only after the first sand boil develops before the normalized data for PPB and PPC start decreasing faster. The sand boils seemed to have allowed the lower portions of the sample to loosen. This could be due to the erosion of particles from the lower portion that then allowed the remaining soil to loosen. As the test progressed the sample continued to heave. This can be seen in Figure 28, where the differential head for the total differential head, PPB, and PPC are sloping downward as the soil loosened as it slowly heaved. The differential pressure in PPA stayed at a constant value because the top portion of the sample had already reached a loosened state.

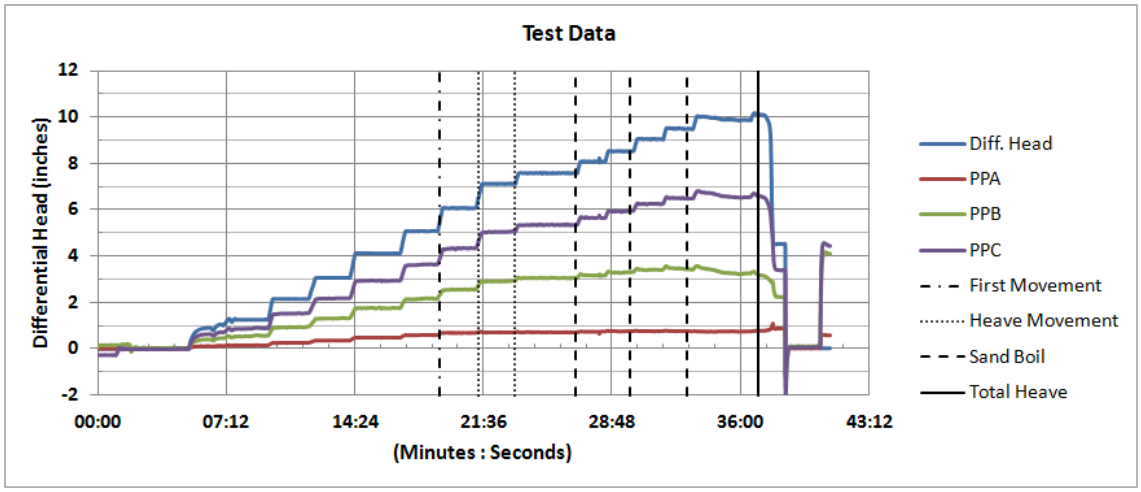

Figure 28. Test data for 20-30 Ottawa sand (6/22/2012).

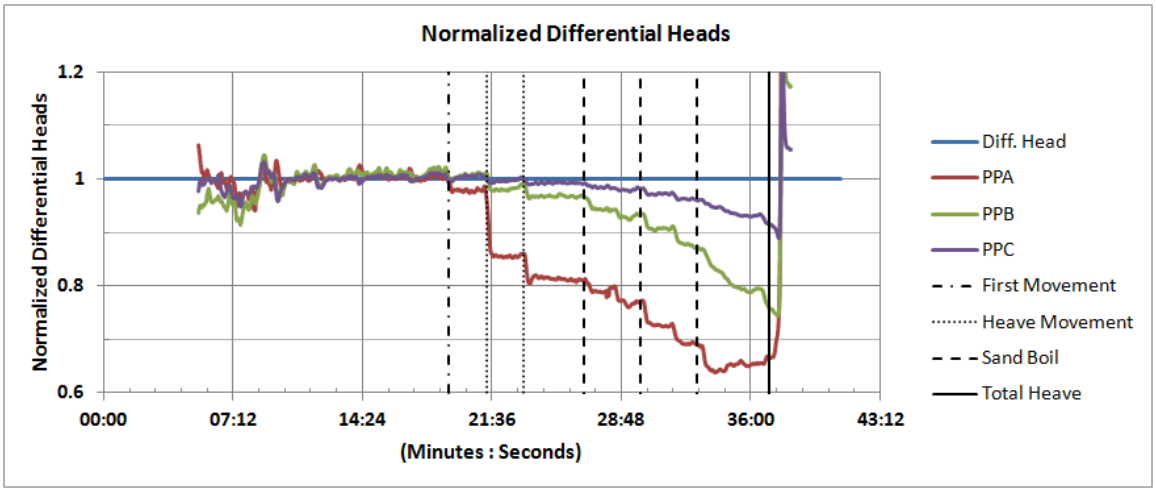

Figure 29. Normalized test data for 20-30 Ottawa sand (6/22/2012).

During the last part of the test where the sample slowly heaves, as the downward progression continues to loosen the top soils rises until it reaches an unstable configuration. The sand sloughs off the sides of the heaved soil, out onto the top lip of the sample holder. The weight of this portion of the sand is then transferred to the sample holder. This removes some of the pressure of the overlaying soils and accelerates the sample into the third stage, total heave and the entire soil sample is heaved upward. The progression of this phenomenon is shown below in Figure 30.

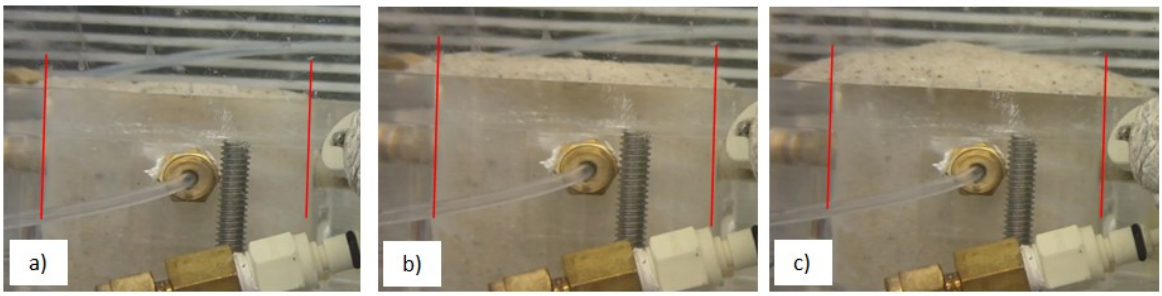

Figure 30. Progression of heave in test 6/22/2012 showing: a) initial heave b) heave spreading out onto sample holder c) just before total heave.

In the test on Graded Angular sand, shown in Figures 31 and 32, the normalized data hovers around a value of 1.0 until the first visible movement and the start of the heave phase. This occurred at a differential head of about 7 inches and about 15 minutes into the test. The normalized data for PPA begins to deviate below a value of 1.0. This initial movement is nearly imperceptible on the video and there is only a small drop in PPA. However, at the next heave movement at a total differential head of 8 inches, the heave movement was larger and there was a large associated drop in the normalized data for PPA.

The normalized data for PPA continues to drop with every associated increase of total differential head. This is due to the continued loosening of the top soil as it

continues to bulge over the top of the sample holder. The normalized data for PPB and PPC did not start deviating from unity until a total differential head of about 9.5 inches was reached. This reflects the downward progression of the loosening of the sand. A sand boil occurred 30 minutes into the test at a total differential head of 11.2 inches, gradient of 2.24. An accompanying drop in the normalized data can be seen in all three pore pressure measurements.

After the second sand boil developed along with a simultaneous heave movement, the normalized data for PPB and PPC started decreasing at a faster rate until the sample reached total heave. Just before the sample reaches total heave both the differential head and the normalized differential head of PPB started to decrease at a rapid rate as the soil particles started moving up and sloughing off the sides of the soil sample. In the normalized data this can be seen as the data for PPA, PPB, and PPC start to return back to unity.

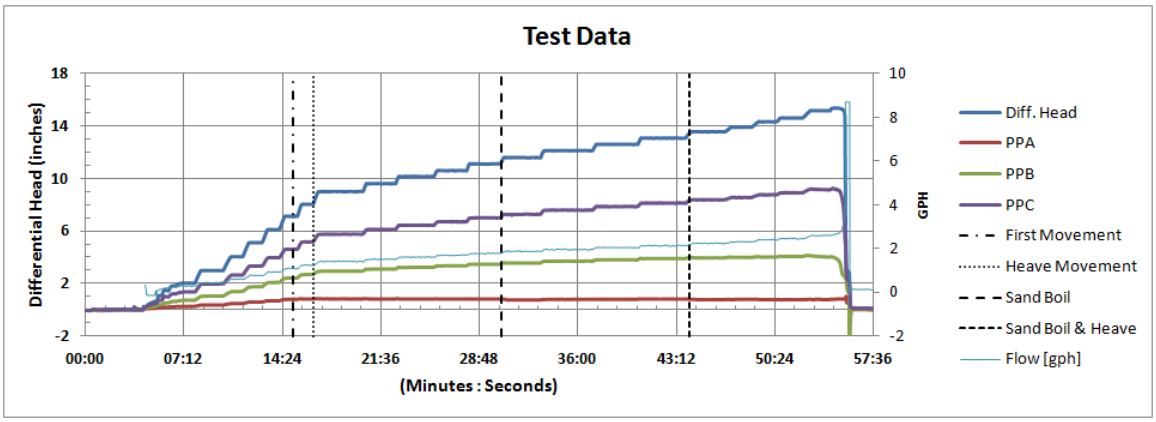

Figure 31. Test data for Graded Angular sand (7/23/2012).

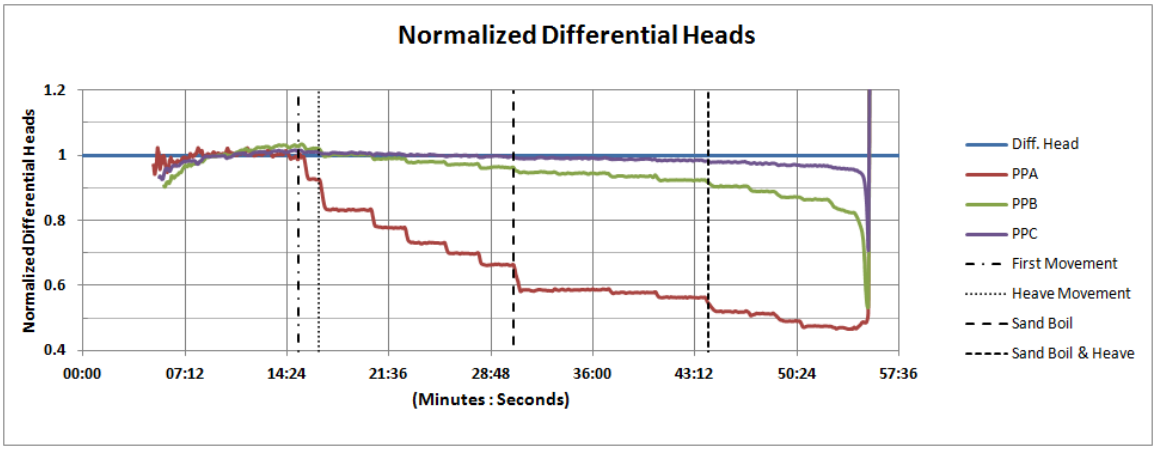

Figure 32. Normalized test data for Graded Angular sand (7/23/2012).

The test on Graded Angular sand, shown in Figures 33 and 34, the normalized data hovers around a value of 1.0 until the first visible movement, which in this case was a sand boil formation on the edge of the sample holder. This occurred at a differential head of about 7 inches, gradient equal to 1.4 and about 11 minutes into the test. The normalized data for PPA begins to deviate below a value of 1.0 at that time. The next sand boil to form occurred at 16 minutes into the test and at a total differential head of 8.6 inches, gradient equal to 1.72. This is accompanied by a larger drop in the normalized data for PPA. There is also a slight deviance in the normalized data of PPB and PPC.

The next drop in normalized data for PPA and PPB occurs when there is a significant heave movement at a total differential head of 9.5 inches, gradient equal to 1.84. After the heave movement the soil loosened enough to allow the differential head measurement at PPA to remain constant even with the continued increases of the total differential head. Normalized test data for PPA, PPB, and PPC continues to drop with

every associated increase of total differential head. This is due to the continued loosening of the top soil as it continues to arch across top of the sample holder.

The third sand boil occurred along with a heave movement at a total differential head of 11.5 inches, gradient equal to 2.3. An accompanying drop in the normalized test data for all three pore pressure measurements occurred as the sand boil developed and the following heave movement. After another increase of half of an inch of total differential head the soil rose and moved outward at a very slow rate as it started to reach total heave in the failure progression. The downward slope of the test data at this stage of the failure progression can be seen in Figure 33, which starts at 33 minutes into the test.

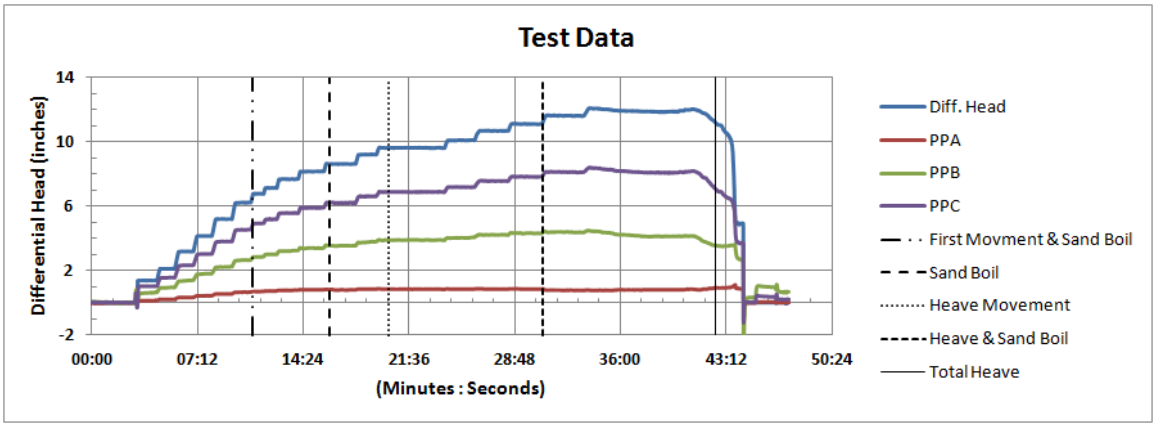

Figure 33. Test data for 20-30 Angular sand (7/26/2012).

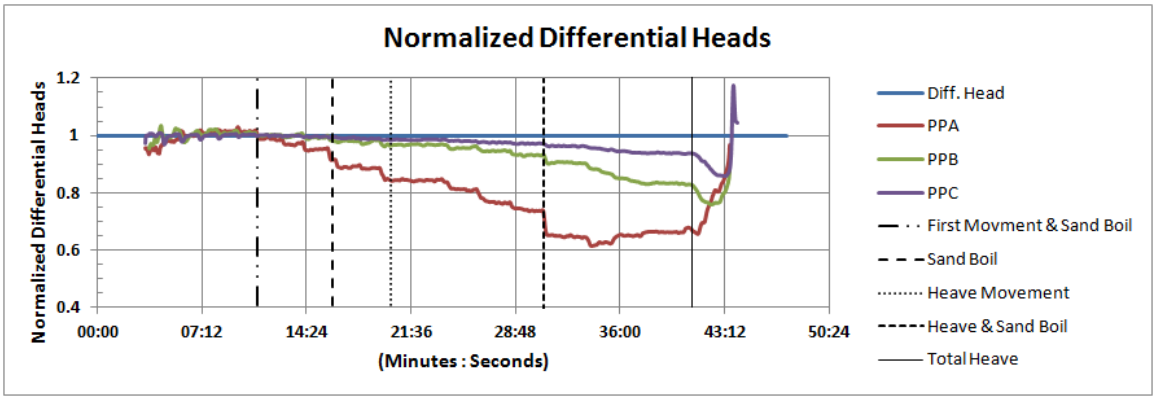

Figure 34. Normalized test data for 20-30 Angular sand (7/26/2012).

The test on Garnet sand, shown in Figures 35 and 36, the normalized data hovers around a value of 1.0 until the first visible movement. This occurred at a differential head of about 9 inches, gradient equal to 1.8 and about 19 minutes into the test. The normalized data for PPA begins to deviate below a value of 1.0 at that time. The next larger drop in the normalized data for PPA occurred when a sand boil formed in the soil sample. This occurred 19.5 minutes into the test, at a total differential head of 9 inches. There is also a slight deviance in the normalized data of PPB.

The subsequent drops in the normalized data for PPA and PPB occur as the sample continues to rise with each increase in differential head. After the heave movements, the soil loosened enough to allow the differential head measurements at PPA to remain constant even with the continued increases of the total differential head. Normalized test data for PPC starts to drop after the occurrence of the noted heave movement indicated in Figure 36. After a differential head of 14.5 inches, gradient of 2.9, the soil sample slowly started to heave until total heave was reached. This is when the normalized data and the test data for PPB start decreasing rapidly.

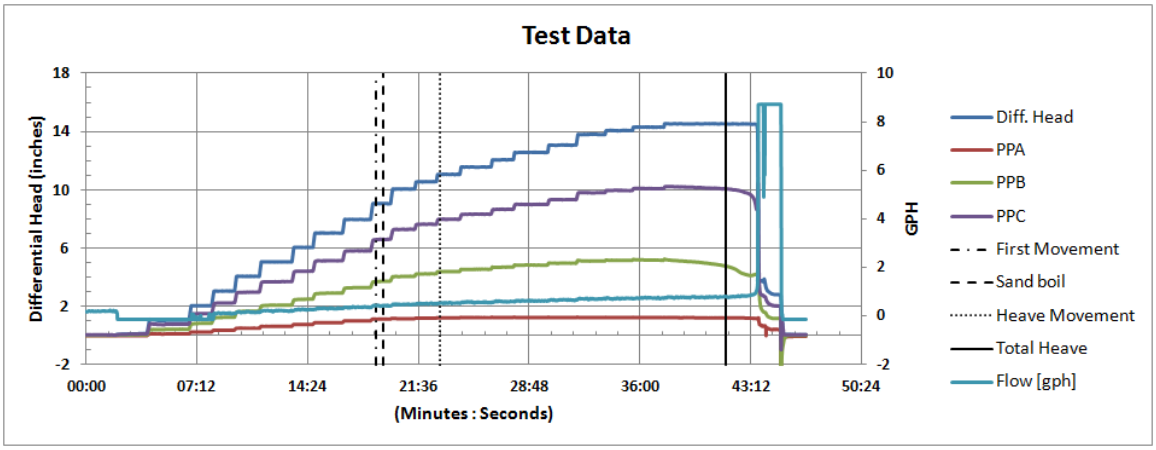

Figure 35. Test data for Garnet sand (8/2/2012).

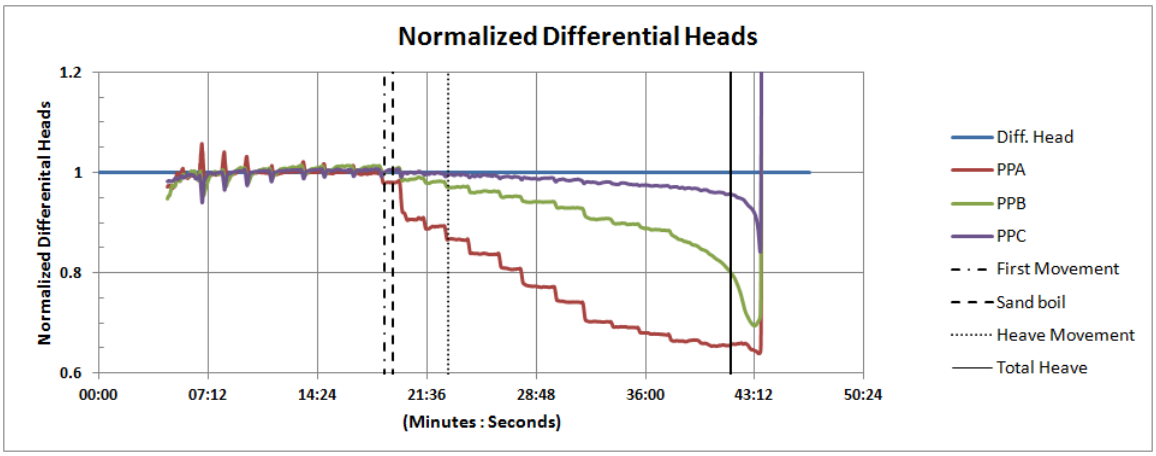

Figure 36. Normalized test data for Garnet sand (8/2/2012).

5.6 Comparison with FEM Modeling

Finite element numerical models were developed for both 20-30 and graded Ottawa sands to validate the theory of the downward progression of loosening of soil. Two models were developed for each type of sand, 1) a model with the top soil loosening and heaving seen in Figure 37 and 2) a model where the soil does not loosen and remains 5 inches tall (no heave model). The model with the top soil loosening was developed by analyzing the recorded videos of the failure progression of the soils. The heights to which the soil raises above the soil sample holder were noted at stages throughout the failure. The differential heads at PPA, PPB, PPC and the total differential head were recorded from the lab data for each of the stages of failure. The PPA, PPB, and PPC values were compared to the total head output in the Slide model at the locations of the pore pressure ports.

The model was produced using soil that is either dense sand or loose sand. The dense sand is a model of the calculated void ratio when the sample is first prepared, e_o.

The loose sand is a model of the calculated void ratio after the sample has completely heaved, e. The soil at the end of the test has been completely heaved and re-deposited in its loosest state in water. The height of the left over soil (the soil that did not heave out of the sample holder) was measured and the soil was dried and weighed. The loose void ratio e, was calculated using this remaining soil. It was estimated that this void ratio would be close to the void ratio of the heaved portion of the sample during the experiment.

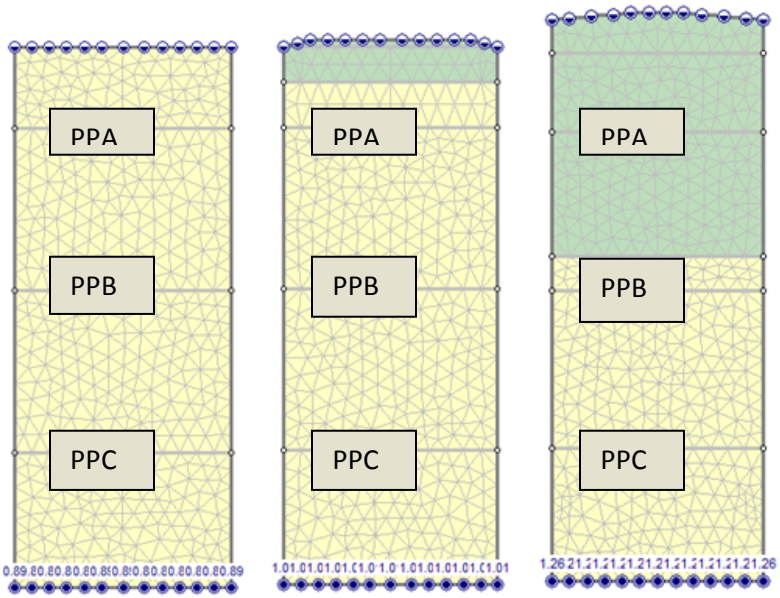

Material Name	Color	Model	KS (ft/s)	K2/K1	K1 Angle (deg)	Soil Type
Dense Sand		Simple	0.009276	1	0	General
Loose Sand		Simple	0.029277	1	0	General

Figure 37. Slide model of downward progression of loosening soil.

The permeability of each state of the soil was calculated using the Kozeny-Carman equation:

$$k = \frac{1}{36} C_s C_l \frac{\gamma_w}{\mu_w} {D_s}^2 \frac{e^3}{1+e} \qquad \text{[Equation 5-1]}$$

where k = hydraulic conductivity (cm/s), C_s = shape factor, C_l = path length factor, Υ_w = unit weight of water(kN/m^3), μ_w = kinematic viscosity of water (m^2/s), D_s = effective particle diameter (mm), e = void ratio (Das, 1983; Holtz and Kovacs, 1981; Rice, 2004). C_s, C_l, Υ_w, μ_w, and D_s are constant for each type of soil. Therefore the equation can be re-written as:

$$k = C\ \frac{e^3}{1+e} \qquad \text{[Equation 5-2]}$$

where the hydraulic conductivity is only a function of the void ratio for the sands and a constant value. Laboratory data for the hydraulic conductivity tests on the 20-30 and graded Ottawa sands are presented in Appendix C.

Two samples for both the 20-30 and the graded Ottawa sands were collected in order to calculate the void ratios and permeabilities of each soil. The void ratios and permeabilities were then used to represent each sample as a whole. The void ratios and permeabilities of each soil are shown below in Table 6. The permeability increased by a factor of about 3 between the original (dense) sand and the loose sand.

Table 6. Void ratio and permeability for Ottawa sands.

	Dense	Loose	Dense Sand		Loose Sand	
Material	**Void Ratio e_o**	**Void Ratio e**	**Permeability k_o [cm/s]**	**Permeability k_o [ft/s]**	**Permeability k [cm/s]**	**Permeability k [ft/s]**
20-30 Ottawa Sand	0.539	0.839	2.83E-01	9.28E-03	8.92E-01	2.98E-02
Graded Ottawa Sand	0.515	0.805	5.04E-02	1.65E-03	1.62E-01	5.30E-03

The depth to which the soil loosened was estimated using following equation:

$$x\frac{1+e}{1+e_o} = x + \Delta x \qquad \text{[Equation 5-3]}$$

where x = depth that the soil loosened, e = loosened void ratio, e_o = original void ratio, and Δx = change in height of the soil sample. This equation estimates the depth x, down

to which the soil would have to loosen, (i.e. larger void ratio; therefore, a larger total volume) in order to have expanded above the top of the soil sample holder a distance Δx.

A model for both graded and 20-30 Ottawa sand samples was created in the finite element computer program Slide. Each model started where the first movement occurred and continued through the failure progression until just before total heave. A video of a laboratory test for both the graded Ottawa and 20-30 Ottawa sand was analyzed and the following Table 7 presents the failure progression established for both samples. These failure progressions were not the same for every test of the same sand, but were used as a general representation of the failure progression to test the theory of downward migration of the loosening of soil during the duration of the laboratory test.

Table 7. Failure progression and height data for graded and 20-30 Ottawa sands.

Graded Ottawa Sand		**20-30 Ottawa Sand**	
Failure Progression	**Height above soil sample holder**	**Failure Progression**	**Height above soil sample holder**
First Movement	-	First Movement	-
Heave Movement	1/64"	Heave Movement	1/16"
Heave Movement	1/32"	Heave Movement	1/16"
Sand Boil	1/16"	Sand Boil	3/16"
Heave Movement	3/16"	Sand Boil	5/16"
Total Heave	5/16"	Total Heave	3/8"

Figures 38 and 39 present the Slide models and results for 20-30 Ottawa sand. Figure 38 shows the progressive heaving and downward progression of the loosening of soil as calculated by Equation 5-3. Figure 39 shows the results from the slide analysis

displaying the differential head at the pore pressure measurement locations. Both figures show the increase in height of the soil above the sample holder.

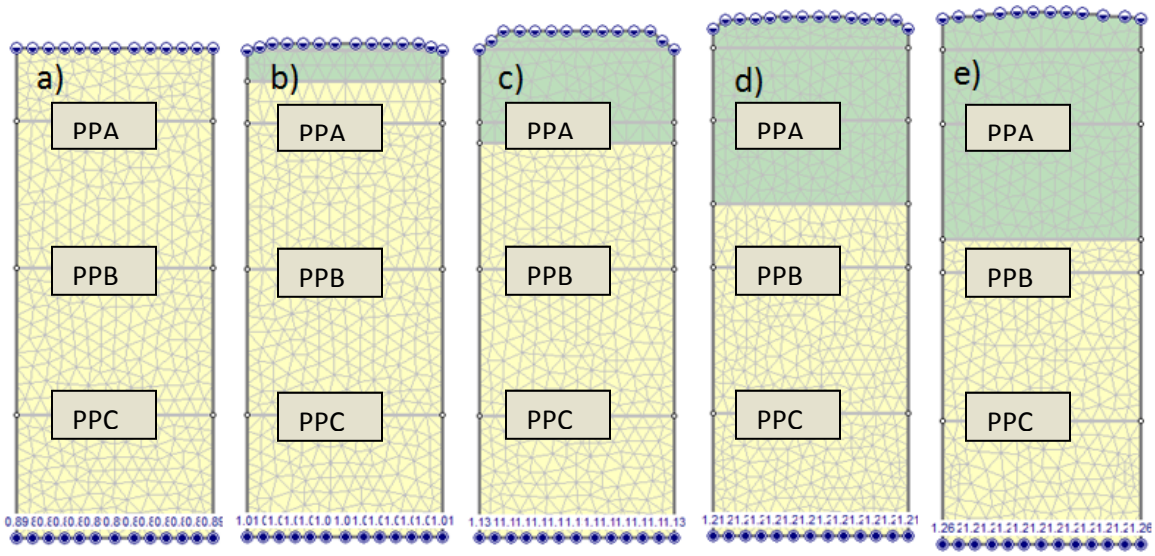

Figure 38. 20-30 Ottawa sand Slide model with a)0 in. b)1/16 in. c)3/16 in. d)5/16 in. e)3/8 in. of heave above sample holder.

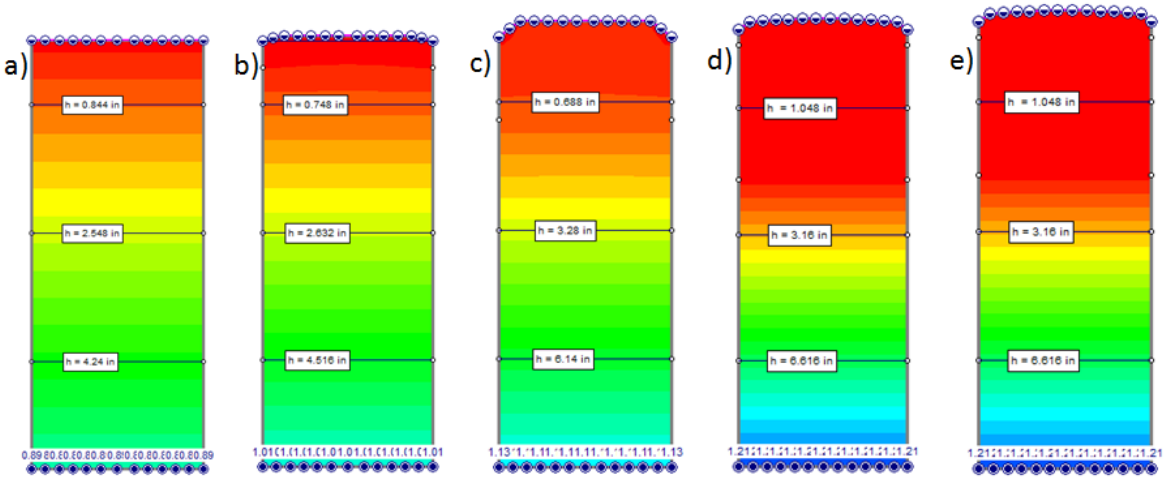

Figure 39. 20-30 Ottawa sand Slide model results with a)0 in. b)1/16 in. c)3/16 in. d)5/16 in. e)3/8 in. of heave above sample holder.

Figure 40 is a graph of Laboratory data, Slide model of downward progression of the loosening of soil, and Slide model where the soil does not heave as the differential head increases (no heave model). The No heave model is a theoretical model of the soil

sample where there is no change in void ratio due to the loosening of soil. It models the differential heads that soil sample would develop at each noted point in the failure progression if there was no loosening of the soil during the test. The results from Slide of the loosening soil model for all three pore pressure measurements are close to the laboratory data. Both sets of data start out following the theoretical Slide model where the sample does not heave (represented by the straight line in the graph). However, as the test proceeded, both sets of data deviate from the theoretical Slide model.

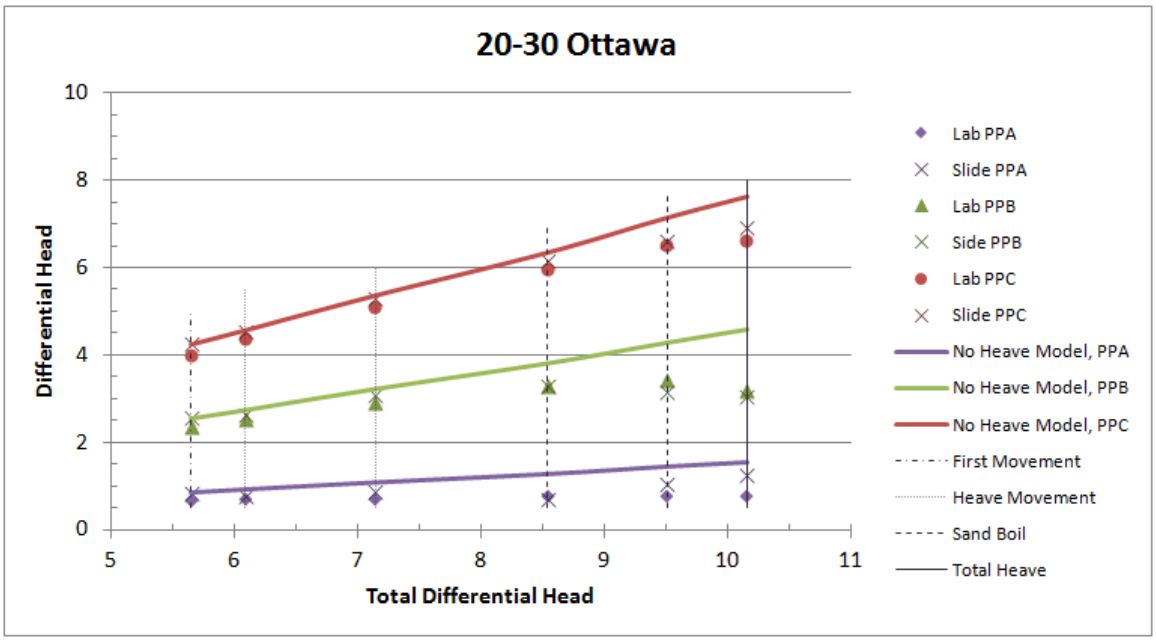

Figure 40. 20-30 Ottawa sand lab data and Slide model comparison.

Figures 41 and 42 present the Slide models for graded Ottawa sand. Figure 41 shows the downward progression of the loosening of soil as calculated by Equation 5-3. Figure 42 shows the results from the slide analysis displaying the differential head at the pore pressure measurement locations. Both figures show the increase in height of the soil above the sample holder.

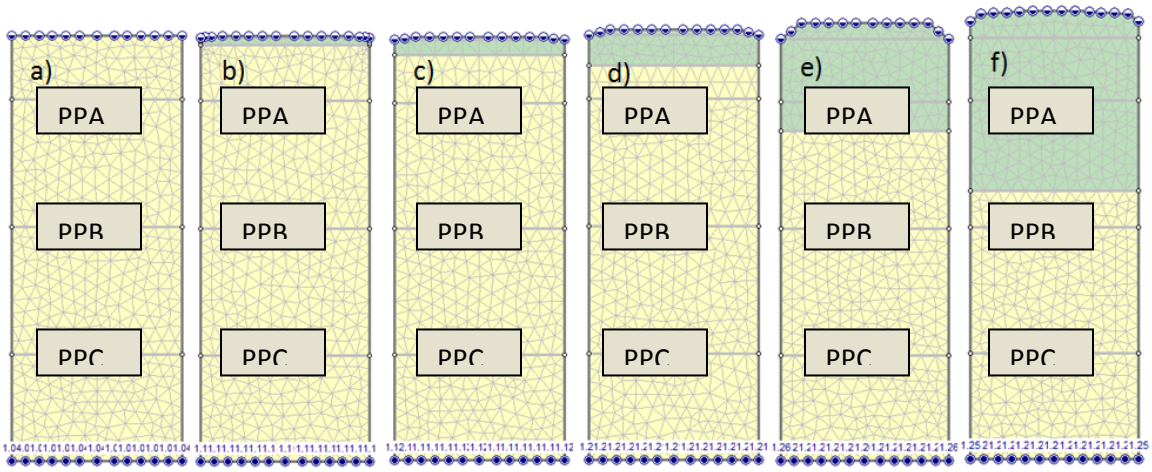

Figure 41. Graded Ottawa Slide model with a)0 in. b)1/64 in. c) 1/32 in. d)1/16 in. e)3/16 in. f)5/16 in. of heave above sample holder.

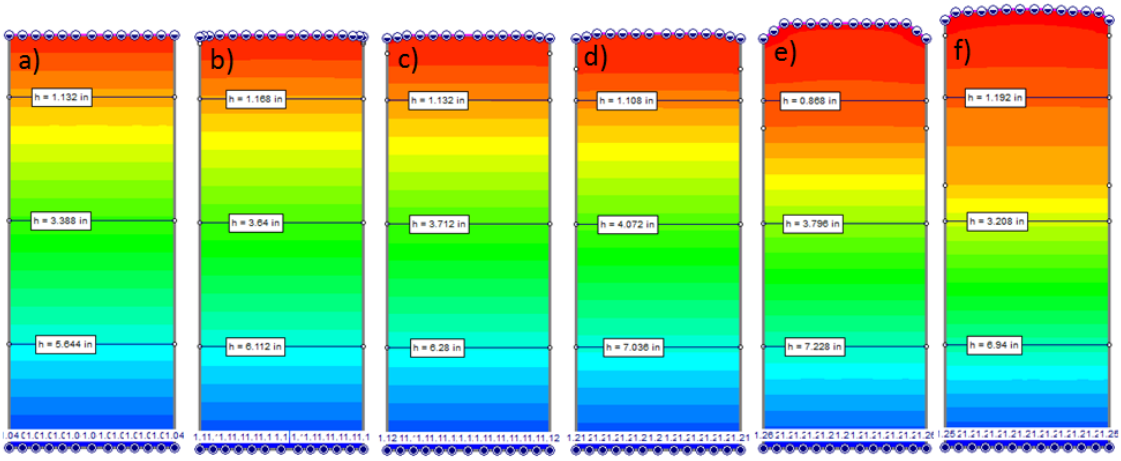

Figure 42. Graded Ottawa Slide model results with a)0 in. b)1/64 in. c) 1/32 in. d)1/16 in. e)3/16 in. f)5/16 in. of heave above sample holder.

Figure 43 is a graph of Laboratory data, Slide model of downward progression of the loosening of soil, and Slide model were the soil does not heave as the differential head increases. The Slide data for all three pore pressure measurements are close to the laboratory data. Both sets of data start out following the theoretical Slide model where the sample does not heave (represented by the straight line in the graph). However, as the test proceeded, both sets of data deviate from the theoretical Slide model. The Slide data is shifted slightly up from the laboratory data. This could be

from a shift in the pore pressure measurement tube being shifted in the soil sample. The tube for the pore pressure measurement is a flexible 1/8” hose that can be moved slightly either up or down depending on how the soil is compacted and the pore pressure lines are connected when the laboratory test is set up.

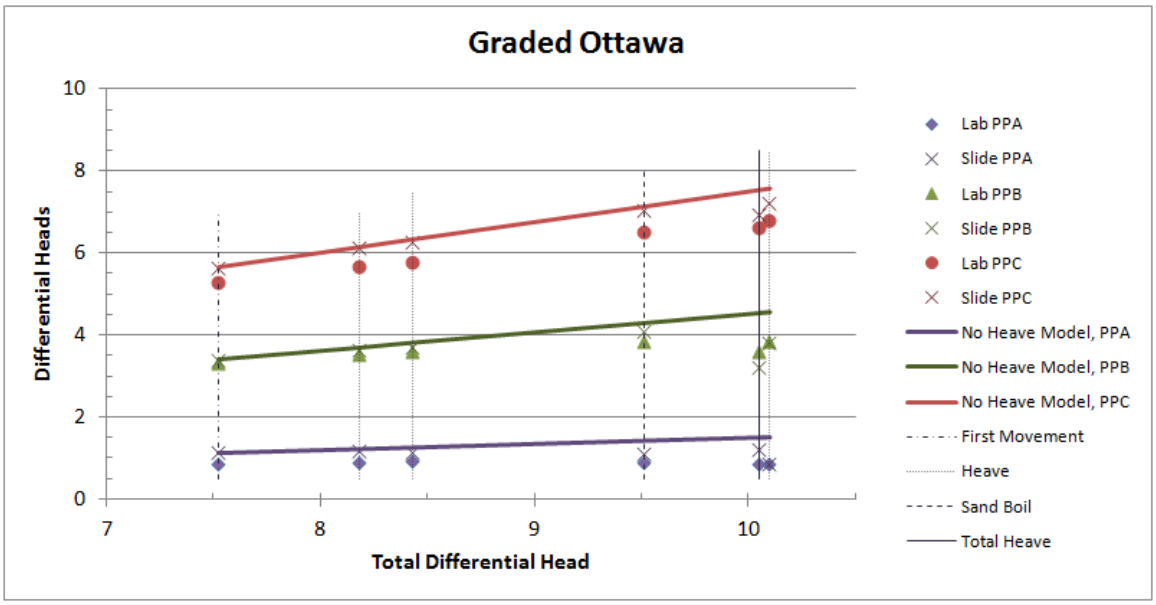

Figure 43. Graded Ottawa sand lab data and Slide model comparison.

Both Figures 40 and 43 support the theory of downward progression of loosing top soils in the failure progression.

CHAPTER 6

SUMMARY AND CONCLUSIONS

The thesis presents the results of laboratory testing to measure critical hydraulic conditions for the initiation of piping in sandy soils and observe the mechanisms associated with the initiation of piping. The laboratory tests were designed to measure hydraulic gradients closer to the microscopic grain size scale as opposed to macroscopic global hydraulic gradient. This was done to gain a better understanding of the piping process on a grain size scale, which is expected to lead to better techniques for predicting initiation of piping erosion with continued research.

Three stages of piping development were identified in the research: initial heave, boil formation, and total heave. Initial heave is thought to be attributed to incipient motion of the soil particles on the surface of the soil sample. As well as an initial loosening of the top soil which increases the permeability due to the increase in void ratio. While the initial and final heave were observed in all tests, sand boils did not form in all tests. Sand boils were more common in graded soil samples than in uniform soils. The development of these various stages is seen in both visual observation and pore pressure instrumentation.

The theory of the downward progression of loosening of soil can be observed in the normalized test data. It was also modeled in Slide, which supported the laboratory test results. The model that included the downward movement of loosening of the top soil matched the lab results.

The effect of different sample holders was evident in the test results. The smooth-sided sample holder modeled the heave mechanism rather than backward erosion piping. Tests using the smooth-sided sample holder produced a narrow band of critical gradients due to the small amount of variation of soil unit weight. The sample holders coated with silicon resulted in tests where the piping progression was observed. These tests resulted in higher critical gradients with a much wider range of values which is attributed to the variability of the soil structure on a grain scale.

Several different soils were tested in the research. The sands varied in grain size, gradation, grain shape, and specific gravity. The test results indicated the following: 1) angular soils showed greater piping resistance, 2) graded soils showed greater piping resistance, and 3) soils with higher specific gravity showed greater piping resistance.

Hydraulic gradients measured in the laboratory research at the formation of piping or sand boils, were higher than past research has presented. This is due to the differences in the laboratory testing. The past research has always measured global hydraulic gradients, across a significantly larger soil sample than the small soil samples used in this research. Past research did not measure the local hydraulic gradients at the seepage exit points that initiated the piping erosion. Also, in past research there have been complex flow paths and geometries at the seepage exit points that made accurate measurements of hydraulic gradients difficult. This research measured the hydraulic gradients across a small soil sample as well as at points within the soil sample in order to measure the hydraulic gradients closer to the microscopic grain size scale needed to understand the piping mechanism.

Because the critical gradient values obtained in these tests are specific to the conditions within the sample holders, they by themselves are of limited value to the general geotechnical engineering community at this time. However, the observations of the progression of piping initiation provide improved understanding of the piping process. This improved understanding is expected to lead to better techniques for predicting initiation of piping erosion with continued research.

REFERENCES

Bligh, W. G. (1910). “Dams, barrages, and weirs on porous foundations.” *Engineering News* 64(26), 708-710.

Bligh, W. G. (1913). “Lessons from the failure of a weir and sluices on porous foundations.” *Engineering News*, 69(6), 266-270.

Das, B. M. (1983). *Advanced soil mechanics*. Hemisphere Publishing Corporation, New York.

Davis, J. (2010). “Herbert Hoover Dike.” *United States Society on Dams Levee Workshop*, November 2-4, Memphis, TN.

de Wit, G. N., Sellmeijer, J. B., and Penning, A. (1981). “Laboratory tests on piping.” *Proceedings: 10th International Conference on Soil Mechanics and Foundation Engineering*, Stockholm, June 1981. Balkema, Rotterdam, 517-520.

Holtz, R. D., and Kovacs, W. D. (1981). *An introduction to geotechnical engineering*. Prentice-Hall, Englewood Cliffs, NJ.

Khilar, K. C., Folger, H. S., and Gray, D. H. (1985). ‘‘Model for piping plugging in earthen structures.’’ *J. Geotech. Engrg., ASCE*, 111(7), 833–846.

Lane, E. W. (1934). “Security from underseepage masonry dams on earth foundations.” *Transactions*, ASCE, 60(4), 929-966.

McCook, D. (2004). A comprehensive discussion of piping and internal erosion failure mechanisms. *Proceedings: The Annual Conference of the Association of State Dam Safety Officials,* Dam Safety 2004, Sept. 26-30, 2004.

Ojha, C. S. P., Singh, V. P., and Adrian, D. D. (2001). “Influence of porosity on piping models of levee failure.” *J. Geotech. Geoenviron. Engr.*, ASCE, 127(12), 1071-1074.

Ojha, C. S. P., Singh, V. P., and Adrian, D. D. (2003). “Determination of critical head in soil piping.” *J. Hydraul. Engr.*, ASCE, 129(7), 511-518.

Rice, J. R., (2004). “A review of methods for estimation of hydraulic conductivity in granular soils based on index testing.” Graduate Seminar at Virginia Tech University.

Richards, K. S., and Reddy, K. R. (2007). “Critical appraisal of piping phenomena in earth Dams.” *Bull. of Engr. Geology and the Environ.*, 66(4), 381-402.

Schmertmann, J. H. (2000). “The non-filter factor of safety against piping through sands.” Geotechnical Special Publication No. 111, *Judgment and innovation*, F. Silva and E. Kavazanjian eds., ASCE, Reston, VA.

Sellmeijer, J. B. (1988). ‘‘On the mechanism of piping under impervious structures.’’ PhD thesis, Technical University, Delft, The Netherlands.

Sellmeijer, J. B., and Koenders, M. A. (1991). ‘‘A mathematical model for piping.’’ *Appl. Math. Modelling*, 15(6), 646–651.

Skempton, A. W., and Brogan, J. M. (1994). “Experiments on piping in sandy gravels.” *Geotechnique,* 44(3), 449-460.

Terzaghi, K. (1943). *Theoretical soil mechanics*. Wiley, New York.

Terzaghi, K., and Peck R. B. (1948). *Theoretical soil mechanics in engineering practice*. Wiley, New York.

Terzaghi, K., Peck, R. B., and Mesri, G. (1996). *Soil mechanics in engineering practice*. John Wiley . New York.

Tomlinson, S. S., and Vaid, Y. P. (2000). “Seepage forces and confining pressure effects on piping erosion,” *Canadian Geotech. J.,* 37, 1-13.

Vroman, N. (2005) “The history of levee design criteria.*” United States Society on Dams Levee Workshop*, Novemeber 2-4, Memphis, TN.

APPENDICES

APPENDIX A

Step by step instructions for the testing procedure:

1. De-air wall tank
    a. Turn on vacuum in sink
    b. Turn on “Fill Cell” on the panel board if Tank 1 is low on water
        i. Turn off “fill cell” before Tank 1 is full so as not to flood the lab
    c. Connect vacuum to the low and high-head reservoirs
        i. Turn on vacuum hose switch on the panel board
    d. Open needle valve on high-head reservoir to fill water from Tank 1
    e. Keep the vacuum on for at least 30 to 60 min before using the water
    f. Close needle valve before overfilling the high-head tank
2. Prepare Soil Sample
    a. Weigh empty sample holder
    b. Fill sample holder with the appropriate sand (use dry raining and vibratory compaction by taping sides while filling)
    c. Weigh full sample holder and record on the “critical gradient calculations” excel sheet
3. Assemble sample holder and pressure cells
    a. Connect the bottom pore pressure lines (PPC)
    b. Place soil sample holder in pressure cells
    c. Place the washers and wing nuts, to secure the soil sample and seal the low and high pressure cells
        i. Tighten the wing nuts to ensure a good seal between cells
    d. Connect other pore pressure measurement lines to the appropriate lines through the lid
        i. Connect far line through the lid to the top pore pressure measurement (PPA)
        ii. Connect middle lid line to the middle pore pressure measurement (PPB)
        iii. Tuck tubes to the back side so there is a clear camera view of the sample
    e. Put the top plate on and secure with washers and wing nuts
        i. Tighten to ensure a good seal
4. Vacuum and C02 through soil sample
    a. Connect the vacuum line to the higher head cell (let full vacuum establish before connecting CO2)

i. When removing vacuum from the higher head reservoir tank, vent both of the reservoirs
    1. Open valve on the high-head reservoir
    2. Bleed air from low-head reservoir carefully so water is not siphoned in to the low-head reservoir and air bubbles do not re-aerate the de-aired water in the high-head reservoir

b. Connect CO2 to top plate of the lower head pressure cell (for ~15 min)
c. Turn on CO2 tank
d. Disconnect CO2 from top cell and turn off CO2 tank after ~15 min.
e. Continue Vacuuming the cell

5. Fill pressure cells with de-aired water
    a. Fill pressure cells from the lower head pressure cell
        i. Remove vacuum line when the water level in the higher head pressure cell reaches the quick connect, so as not to vacuum water
    b. Let the pore pressure lines fill with water before bleeding any remaining air to completely fill the low-head pressure cell
6. Bleeding pore pressure Lines
    a. Leave the low-head pressure cell connected to the high-head reservoir
    b. Bleed the pore pressure lines one at a time
    c. Bleed out remaining air in top of low-head pressure cell
7. Finish setting up Test
    a. Connect the low-head reservoir to the low-head pressure cell
    b. Connect the high-head reservoir to the high-head pressure cell
8. **Connecting Pressure Transducers –** ***watch differential pressures (or #2) the whole time to not over-pressurize the differential pressure transducers***
    a. Open bleed valves on pressure transducers
    b. Open bypass valve on the outside of the water cells
    c. Connect the negative side of the pressure transducers to the low-head pressure cell
    d. Connect the positive side of the pressure transducers to the high head pressure cell
    e. Bleed the positive and negative lines connected to the pressure transducers
        i. Open valves to high-head reservoir to provide flow
        ii. <u>After done bleeding transducer lines, close valve to large tank and open bleed valve in the top plate to relieve pressure (slowly)</u>

f. Disconnect the positive side of the pressure transducers that will be used to measure the pore pressures (quick connects)
g. Connect the pore pressure lines to the positive side of the pressure transducers
    i. Top pore pressure measurement (PPA) to Pressure transducer #3
    ii. Middle pore pressure measurement (PPB) to Pressure Transducer #2
    iii. Bottom pore pressure measurement (PPC) to Pressure Transducer #1
h. Close bleed valves on pressure transducers

9. Zeroing the Pressure Transducers
    a. Open Logger Net on computer (on the desktop)
    b. Turn on the power to the data logger
    c. Re-send the piping program
    d. Click the "Connect" button
    e. Set the "Table Start" value to 1 to start collecting the data
    f. Open graph 1 to view the pressure transducers
    g. Zero the pressure transducers using the demodulator & Logger Net
    h. Collect the data by clicking "Collect Now"
    i. Click the "Disconnect" button to stop collecting data (where the "connect" button was)
    j. Reset the "Table Start" value to zero
    k. Open My computer→ C drive → Campbell Scientific → Logger net → CR1000 data, right click and delete the data.
10. Pressurize the reservoirs and apply back pressure for saturation
    a. Make sure the bypass valve is open
    b. Open all water valves to the high-head reservoir (not bleed valves)
    c. Open the valve between the low-head reservoir and the clear hose, but not the valve between the clear hose and the low-head pressure cell
    d. Connect the "wall tanks" line to Panel 1 and pressurize the reservoirs up to 15 psi slowly
    e. Re-zero the transducers just using the demodulator display (if needed)
11. Starting the Test
    a. Set up camera side view
    b. Put on electronic pulse counter
    c. Reconnect the data logger by clicking the "connect" button on the connect screen
    d. Start Video

e. Set “Zero LCDM” and “Table Start” values equal to 1 (in that order)
f. RE-zero the pressure transducers using the demodulator (if needed)
g. After zero’s are established open top cell valve
h. Close the bypass valve

12. Proceed with test
    a. Raise the Mariotte tube in one inch increments
    b. Wait to raise head until the pore pressure readings level out (~1.5 to 3 min)
    c. After reaching a certain point (depending on the type of sand) start raising in half inch increments
    d. If any sand boils form, stop raising the differential head and wait for at least 1.5 min before raising again
13. At failure (total heave)
    a. Wait for about a minute before closing the valves after the sand has heaved
    b. Stop camera recording at this point
    c. Keep collecting data until the pressure transducers readings level off (~3 to 5 min)
    d. Collect the data by clicking the “Collect Now” button in the “Connect Screen”
    e. Open My computer→ C drive → Campbell Scientific → Logger net → CR1000 data, right click and open with Notepad
    f. Save as → Desktop → Mandie → Exp Data → Text Files → “date type of sand”
14. Clean up
    a. Close logger net
    b. Turn off data logger power
    c. Turn off valves connecting the reservoirs and the pressure cells
    d. Vent reservoirs
    e. Open Bypass valve
    f. Slowly Vent the pressure cells to relieve pressure
        i. Open valve between the low-head reservoir and the clear hose
        ii. Slowly open the valve between the lower pressure cell and the clear hose while watching pressure for pressure transducer #2
        iii. Try not to let the pressure go beyond + or -20
    g. Open bleed valves on pressure transducers
    h. After pressure is dissipated, disconnect the pore pressure lines and re-connect the positive pressure lines (the ones in parallel)

i. Disconnect the pressure transducer pressure lines from the pressure cells
j. Disconnect water supplies from water cell
k. Drain water from the small wall tank
l. Drain water from the water cells
m. Take top plate off and disconnect pore pressure lines
n. Take the pressure cell to sink and wash out sand into a # 200 sieve
o. Remove the sample holder from water cell
p. Copy Video from camera to external hard drive

APPENDIX B

Complete table of tests conducted in this research.

Slicon Sided - First Test Runs

Date	Type	$I_c = \gamma_b/\gamma_w$	γ_b dry	First Visible Movement	i	Sand Boil	i	Total Heave	i	Failure Description	Video #
8/4/2011	Ottawa Sand 20-30	1.066	106.99	6.30	1.26	-		7.0	1.40	Heave	112
8/5/2011	Ottawa Sand 20-30	1.070	107.41	6.70	1.34	-		7.2	1.44	Heave	113
8/8/2011	Ottawa Sand 20-30	1.069	107.28	6.30	1.26	-		6.8	1.36	Heave	114
8/10/2011	Ottawa Sand 20-30	1.056	106.05	6.60	1.32	-		6.9	1.38	Heave	115
8/11/2011	Ottawa Sand 20-30	1.064	106.78	6.90	1.38	-		7.2	1.44	Heave	116
8/12/2011	Ottawa Sand 20-30	1.054	105.86	6.70	1.34	-		7	1.40	Heave, but top was already l	118
8/12/2011	Ottawa Sand 20-30	1.051	105.57	6.80	1.36	-		7.3	1.46	Heave	119
8/15/2011	Ottawa Sand 20-30	1.045	104.89	6.80	1.36	6.8	1.36	7.1	1.42	Heave, but there were small	120
8/15/2011	Ottawa Sand 20-30	1.042	104.60	6.90	1.38	-		7.7	1.54	Heave	121
9/26/2011	Ottawa Sand 20-30	105.203	1.05	7.90	1.58	-		8.9	1.78	Heave	141
9/26/2011	Ottawa Sand 20-31	105.445	1.05	7.00	1.40	-		7.9	1.58	Heave	142 + 143
9/27/2011	Ottawa Sand 20-32	105.688	1.05	7.00	1.40	-		7.8	1.56	Heave	144 +145
8/17/2011	Ottawa Sand Graded	1.055	105.93	7.30	1.46	7.3	1.46	8.8	1.76	Small pipe on edge @ 7.3, th	122
8/18/2011	Ottawa Sand Graded	1.053	105.69	6.50	1.30	-		8	1.60	Heave	123
8/22/2011	Ottawa Sand Graded	1.050	105.45	6.80	1.36	-		7.3	1.46	Heave	124
8/25/2011	Ottawa Sand Graded	1.053	105.69	7.20	1.44	-		8.2	1.64	Heave	125 + 126
8/29/2011	Ottawa Sand Graded	1.041	104.48	7.80	1.56	-		9.5	1.90	Heave, movement at the fro	129
9/8/2011	Ottawa Sand Graded	1.058	106.17	6.80	1.36	-		7.8	1.56	Heave, air bubbles came out	131
9/12/2011	Ottawa Sand Graded	1.074	107.87	6.40	1.28	-		9.0	1.80	Heave	132
9/13/2011	Ottawa Sand Graded	1.062	106.66	6.70	1.34	-		9.2	1.84	Heave	133
9/14/2011	Ottawa Sand Graded	1.070	107.38	6.10	1.22	-		7.8	1.56	Heave	134
9/19/2011	Ottawa Sand Graded	1.079	108.35	5.90	1.18	7.7	1.54	8.5	1.70	2 sand boils between 7.7 - 8.3	136
9/21/2011	Ottawa Sand Graded	1.070	107.38	6.10	1.22	7.3	1.46	7.8	1.56	Sand Boil at 7.3, Heave at 7.8	138
9/22/2011	Ottawa Sand Graded	1.065	106.90	6.30	1.26	-		9	1.80	Heave	139
9/22/2011	Ottawa Sand Graded	1.077	108.11	5.40	1.08	-		8.5	1.70	Heave	140

Silicon Sided - Before Flow meter and other instrumentation

Date	Type	$I_c = \gamma_b/\gamma_w$	γ_b dry	First Visible Movement	i	Sand Boil	i	Total Heave	i	Failure Description	Video #
10/10/2011	Garnet Sand (clean)	1.473	123.87	9.00	1.80	13.60	2.72	15.50	3.10	Small Piping in middle, then	154
10/12/2011	Garnet Sand (clean)	1.444	121.44	9.50	1.90	-		10.70	2.14	Heave	155
10/18/2011	Garnet Sand (clean)	1.435	120.72	8.00	1.60	-		15.00	3.00	Heave	162
11/18/2011	Garnet Sand (clean) Loose	1.222	102.78	5.30	1.06	5.60	1.12	5.80	1.16	Piping at edge, then heave	191+192
11/21/2011	Garnet Sand (clean) Loose	1.237	103.99	5.80	1.16	5.80	1.16	6.50	1.30	Piping begins@5.8. Another	193
11/21/2011	Garnet Sand (clean) Loose	1.260	105.93	6.30	1.26	-		6.90	1.38	Heave	194
12/7/2011	Garnet Sand (clean) Loose	1.277	107.36	7.60	1.52	7.60	1.52	8.40	1.68	Piping at 7.6, Heave at 8.4	204+205
12/8/2011	Garnet Sand (clean) Loose	1.295	108.92	5.30	1.06	5.30	1.06	8.10	1.62	Small pipe at 5.3, Large Pipe	206
12/8/2011	Garnet Sand (clean) Loose	1.303	109.55	6.50	1.30	6.50	1.30	8.60	1.72	Small Pipe at 6.5, Heave at 8.	207
10/12/2011	Garnet Sand (dried)	1.444	121.44	8.20	1.64	-		12.10	2.42	Heave	156
10/13/2011	Garnet Sand (dried)	1.464	123.14	9.00	1.80	-		13.90	2.78	Heave	157
10/7/2011	Garnet Sand (tub)	1.375	115.65	6.20	1.24	7.80	1.56	10.50	2.10	PIPED!Back edge, progressed	152
10/14/2011	Garnet Sand (tub)	1.424	119.75	8.60	1.72	11.10	2.22	12.20	2.44	Piping in middle @11.1, enla	158
10/17/2011	Garnet Sand (tub)	1.441	121.20	8.00	1.60	11.10	2.22	12.50	2.50	Piping @ 11.1, larger 2nd pip	159
10/17/2011	Garnet Sand (tub)	1.453	122.17	8.30	1.66	-		14.00	2.80	Heave, looked like pipe form	161
11/16/2011	Garnet Sand (tub) Loose	1.185	0.42	5.80	1.16	-		5.80	1.16	Heave	188
11/17/2011	Garnet Sand (tub) Loose	1.185	0.42	5.30	1.06	-		5.40	1.08	Heave	189+190
10/19/2011	Garnet Sand w/2% Kaolinite Clay	1.375	115.63	7.00	1.40	7.00	1.40	-		Small Pipe began @ 7, Large	164
10/27/2011	Garnet Sand w/2% Kaolinite Clay	1.29	105.45	6.10	1.22	6.10	1.22	-		Piping: 3 small independent	172
10/31/2011	Garnet Sand w/2% Kaolinite Clay	1.395	117.32	5.40	1.08	5.40	1.08	-		Piping Began @ 5.4, 2nd sand	174
11/28/2011	Garnet Sand w/2% Kaolinite Clay (Loose)	1.220	102.58	5.00	1.00	-		6.80	1.36	Heave	196
11/28/2011	Garnet Sand w/2% Kaolinite Clay (Loose)	1.176	98.90	4.90	0.98	4.90	0.98	5.90	1.18	Sand Boil on left edge at 4.90	195
9/30/2011	Ottawa Sand 20-30	1.038	104.23	6.20	1.24	-		7.80	1.56	Heave	146
10/4/2011	Ottawa Sand 20-30	1.045	104.96	6.50	1.30	-		8.25	1.65	Heave	147
10/5/2011	Ottawa Sand 20-30	1.038	104.23	5.90	1.18	-		7.60	1.52	Heave	148
11/12/2011	Ottawa Sand 20-30 (loose)	0.932	93.57	4.60	0.92	-		4.60	0.92	Heave	185
11/15/2011	Ottawa Sand 20-30 (loose)	0.937	94.05	4.40	0.88	4.60	0.92	4.60	0.92	Piping then Heave a couple n	186
11/16/2011	Ottawa Sand 20-30 (loose)	0.937	94.05	4.80	0.96	4.80	0.96	4.80	0.96	Piping then Heave a couple n	187
12/9/2011	Ottawa Sand 20-30 (loose)	0.952	95.58	4.10	0.82	4.10	0.82	4.80	0.96	Small Pipe at edge at 4.1; exp	208+209
12/9/2011	Ottawa Sand 20-30 (loose)	0.947	95.09	4.00	0.80	4.00	0.80	4.70	0.94	Small Pipe before Heave	210
12/13/2011	Ottawa Sand 20-30 (loose)	0.948	95.13	4.30	0.86	4.30	0.86	4.95	0.99	Small Pipe before Heave; san	211
10/5/2011	Ottawa Sand Graded	1.055	105.93	6.40	1.28	-		8.25	1.65	Heave	149
10/7/2011	Ottawa Sand Graded	1.050	105.45	6.50	1.30	7.00	1.40	7.90	1.58	Pipe, on left edge	151
11/10/2011	Ottawa Sand Graded (loose)	0.893	89.69	4.60	0.92	-		4.70	0.94	Heave	182
11/11/2011	Ottawa Sand Graded (loose)	0.932	93.57	4.80	0.96	-		5.20	1.04	Heave	183
11/14/2011	Ottawa Sand Graded (loose)	0.915	91.87	4.60	0.92	-		4.80	0.96	Heave	184
12/2/2011	Ottawa Sand Graded (loose)	1.007	101.08	5.90	1.18	7.10	1.42	7.50	1.50	Piping at 7.3 then Heave	199
12/2/2011	Ottawa Sand Graded (loose)	1.002	100.60	5.20	1.04	5.20	1.04	6.60	1.32	Small Pipe begins at 5.2, exp	200
12/6/2011	Ottawa Sand Graded (loose)	0.963	96.72	4.70	0.94	4.70	0.94	5.30	1.06	Piping on edges begins at 4.7	201
12/6/2011	Ottawa Sand Graded (loose)	0.963	96.69	4.10	0.82	4.10	0.82	5.80	1.16	Piping Begins at 4.1, expands	202
10/25/2011	Ottawa Sand Graded with ~1.5% Kaolinite Clay	1.041	104.48	5.00	1.00	7.30	1.46	-		Fines washed out at 5.0, Pipi	166
10/31/2011	Ottawa Sand Graded with ~1-2% Kaolinite Clay	1.05	105.45	7.30	1.46	7.30	1.46	8.00	1.60	Piping Begins. Expands at 8.0	173
10/19/2011	Ottawa Sand Graded with 2% Kaolinite Clay	1.026	103.02	1.00	0.20	5.00	1.00	10.50	2.10	Piping of fines began at 5.0. M	163
10/26/2011	Ottawa Sand Graded with 2% Kaolinite Clay	1.019	102.29	5.00	1.00	8.10	1.62	-		Piping Began	168
10/26/2011	Ottawa Sand Graded with 2% Kaolinite Clay	1.048	105.20	4.60	0.92	8.10	1.62	12.40	2.48	Fines washing out @ 4.6 and	169
11/29/2011	Soda Lime Glass Beads Ottawa Graded	0.952	97.69	3.10	0.62	3.10	0.62	5.50	1.10	Piping (edges at 3.10, middle	197
11/30/2011	Soda Lime Glass Beads Ottawa Graded	0.959	98.42	4.00	0.80	4.00	0.80	-		Piping @ 4.0, larger sand boil	198
11/4/2011	Soda Lime Glass Beads (0.40 mm)	0.905	92.84	5.00	1.00	5.00	1.00	5.00	1.00	Piped then Heaved	178
11/10/2011	Soda Lime Glass Beads (0.40 mm)	0.905	92.84	5.20	1.04	-		5.60	1.12	Heave	181
11/4/2011	Soda Lime Glass Beads (1.00 mm)	0.910	93.33	4.30	0.86	4.30	0.86	-		Piping!	177
11/9/2011	Soda Lime Glass Beads (1.00 mm)	0.912	93.57	5.10	1.02	-		6.00	1.20	Heave	180
11/3/2011	Soda Lime Glass Beads (2.00 mm)	0.907	93.08	3.20	0.64	-		5.60	1.12	Heave	176
11/8/2011	Soda Lime Glass Beads (2.00 mm)	0.907	93.08	5.40	1.08	6.80	1.36	-		Piping Begins @ 6.8, didn't co	179

Silicon Sided - Flow Meter and Transducers in Parallel

Date	Type	$I_c = \gamma_b/\gamma_w$	$\gamma_{b\ dry}$	First Visible Movement	i	Sand Boil	i	Total Heave	i	Failure Description	Video #
2/9/2012	Angular # 16	0.93	93.57	5.10	1.02	-		11.00	2.20	Heave	230
2/10/2012	Angular # 16	0.92	92.36	5.20	1.04	-		7.70	1.54	Heave	232
2/13/2012	Angular # 16	0.92	92.84	8.40	1.68	-		11.80	2.36	Heave	233
2/14/2012	Angular # 16	0.95	95.26	7.40	1.48	-		12.30	2.46	Heave	234
2/14/2012	Angular # 16	0.92	92.60	5.00	1.00	-		11.10	2.22	Heave	235
2/16/2012	Angular Sand 20-30	0.89	88.96	6.80	1.36	-		10.50	2.10	Heave	236
2/22/2012	Angular Sand 20-30	0.89	88.96	8.10	1.62	-		10.50	2.10	Heave	237-238
2/23/2012	Angular Sand 20-30	0.88	88.23	7.80	1.56	-		10.15	2.03	Heave	240+241
2/24/2012	Angular Sand 20-30	0.89	88.96	6.00	1.20	-		10.40	2.08	Heave	242
2/27/2012	Angular Sand 20-30	0.89	89.20	5.95	1.19	-		10.60	2.12	Heave	243
2/28/2012	Angular Sand 20-30	0.88	88.72	6.70	1.34	-		10.00	2.00	Heave	244
2/29/2012	Angular Sand 20-30	0.88	88.48	7.10	1.42	-		10.20	2.04	Heave	245
3/6/2012	Angular Sand Graded	0.92	92.36	5.50	1.10	8.00	1.60	13.60	2.72	Movement, Piping, Heave	247
3/7/2012	Angular Sand Graded	0.92	92.84	4.30	0.86	9.00	1.80	13.80	2.76	Movement, Piping, more pip	248
3/9/2012	Angular Sand Graded	0.92	92.84	6.40	1.28	7.50	1.50	14.40	2.88	Movement, Piping, more pip	250
3/10/2012	Angular Sand Graded	0.93	93.57	5.90	1.18	9.30	1.86	14.60	2.92	Movenemt, Piping (edge), m	251
2/3/2012	Garnet Sand (clean)	1.38	115.87	7.90	1.58	11.40	2.28	11.85	2.37	Piping then heave	225
2/6/2012	Garnet Sand (clean)	1.36	114.41	9.00	1.80	9.00	1.80	9.80	1.96	Piping then heave	226
2/7/2012	Garnet Sand (clean)	1.39	116.50	8.20	1.64	-		10.70	2.14	Heave	227
2/7/2012	Garnet Sand (clean)	1.45	121.69	3.70	0.74	-		12.00	2.40	Heave	228
2/8/2012	Garnet Sand (clean)	1.42	119.02	9.40	1.88	-		13.30	2.66	Heave	229
2/10/2012	Garnet Sand (clean)	1.40	117.81	7.40	1.48	-		10.83	2.17	Heave	231
2/29/2012	Garnet Sand w 2% Kaolinite Clay	1.38	116.16	4.00	0.80	10.00	2.00	11.00	2.20	Heave, Piping, Total Heave	246
3/5/2012	Garnet Sand w 2% Kaolinite Clay	1.37	115.14	5.00	1.00	9.50	1.90	11.60	2.32	Piping, Heave	-
1/31/2012	Ottawa Sand 20-30	1.01	101.57	4.80	0.96	-		8.70	1.74	Heave	220
1/31/2012	Ottawa Sand 20-30	1.05	105.45	6.50	1.30	-		8.90	1.78	Heave	221
2/1/2012	Ottawa Sand 20-30	1.05	105.20	6.50	1.30	-		8.50	1.70	Heave	222
2/2/2012	Ottawa Sand 20-30	1.04	104.39	6.40	1.28	-		7.80	1.56	Heave	223
1/25/2012	Ottawa Sand Graded	1.02	102.54	8.20	1.64	8.20	1.64	10.30	2.06	Piping around edges, then he	215
1/26/2012	Ottawa Sand Graded	0.97	96.93	6.00	1.20	-		8.01	1.60	Heave	216
1/26/2012	Ottawa Sand Graded	1.03	103.51	6.20	1.24	6.20	1.24	9.70	1.94	Piping around edges, then he	217
1/27/2012	Ottawa Sand Graded	1.02	102.05	6.00	1.20	-		7.50	1.50	Heave	218
1/30/2012	Ottawa Sand Graded	0.99	99.55	7.10	1.42	7.50	1.50	8.00	1.60	Piping around edges, then he	219
2/2/2012	Ottawa Sand Graded	1.02	102.54	4.90	0.98	6.00	1.20	7.00	1.40	Piping around edges, then he	224

Silicon Sided and Fully Instrumented - Flow Meter and Pore Pressure Measurements

Date	Type	$I_c = \gamma_b/\gamma_w$	$\gamma_{b\ dry}$	First Visible Movement	i	Sand Boil	i	Total Heave	i	Failure Description	Video #
3/29/2012	Ottawa Sand Graded	1.07	107.63	7.00	1.40	7.00	1.40	9.50	1.90	Piping in middle, then edge,	253
3/30/2012	Ottawa Sand Graded	1.07	107.63	7.20	1.44	7.20	1.44	10.30	2.06	Piping@ 7.2, 8.4, then heave	254
4/4/2012	Ottawa Sand Graded	1.07	107.87	6.90	1.38	6.90	1.38	10.10	2.02	Piping@ 6.9, 7, 7.7, then heav	256+257
4/5/2012	Ottawa Sand Graded	1.08	108.60	5.40	1.08	5.40	1.08	10.50	2.10	sand boil in middle @ 5.4, 2n	258
4/6/2012	Ottawa Sand Graded	1.06	106.90	7.50	1.50	10.00	2.00	10.00	2.00	Heave, piping around edges	259
4/9/2012	Ottawa Sand Graded	1.07	107.14	7.10	1.42	-		10.70	2.14	Heave, no piping	260
4/12/2012	Ottawa Sand Graded	1.07	107.82	7.00	1.40	9.20	1.84	12.20	2.44	Piping in center starting arou	262
4/13/2012	Ottawa Sand Graded	1.09	109.32	7.00	1.40	7.30	1.46	10.70	2.14	Movement started at 7.0, Pip	263 + 264
4/17/2012	Ottawa Sand Graded	1.08	108.11	6.60	1.32	9.30	1.86	10.20	2.04	Heave, leak in PPC	265
7/9/2012	Ottawa Sand Graded	1.083	108.71	7.20	1.440	8.50	1.700	10.75	2.150		297
4/10/2012	Ottawa Sand 20-30	0.942	94.54	6.30	1.26	8.70	1.74	10.00	2.00		261
4/18/2012	Ottawa Sand 20-30	1.014	101.81	6.40	1.28	8.90	1.78	9.50	1.90	Movement@6.4, Piping arou	266
4/23/2012	Ottawa Sand 20-30	1.067	107.14	7.20	1.44	7.50	1.50	9.30	1.86	Movement@7.2, Boil @7.5 &	268
4/24/2012	Ottawa Sand 20-30	1.067	107.14	6.10	1.22	8.60	1.72	9.10	1.82	Movement @ 6.1, sand boil c	269
4/25/2012	Ottawa Sand 20-30	1.082	108.60	6.00	1.20	8.00	1.60	9.80	1.96	Piping around edges; Heave	270
4/26/2012	Ottawa Sand 20-30	1.074	107.87	6.20	1.24	8.10	1.62	9.60	1.92	Movement @ 6.2, Sand boil c	271
4/27/2012	Ottawa Sand 20-30	1.072	107.63	6.10	1.22	8.00	1.60	10.30	2.06	Movement @ 6.1, San dBoil@	272
5/16/2012	Ottawa Sand 20-30	1.069	107.32	7.50	1.50	7.50	1.50	8.50	1.70		281+282
6/4/2012	Ottawa Sand 20-30	1.059	106.34	7.50	1.50	9.00	1.80	9.40	1.88		283
6/5/2012	Ottawa Sand 20-30	1.067	107.10	6.00	1.20	9.00	1.80	9.90	1.98		284+285
6/6/2012	Ottawa Sand 20-30	1.069	107.34	9.00	1.80	-		10.50	2.10	no pipe	286
6/7/2012	Ottawa Sand 20-31	1.067	107.10	5.25	1.05	7.09	1.42	10.00	2.00		287
6/18/2012	Ottawa Sand 20-30	1.073	107.76	7.50	1.50	8.50	1.70	10.00	2.00		288+289
6/19/2012	Ottawa Sand 20-30	1.266	108.20	6.01	1.20	8.50	1.70	10.30	2.06		290
6/21/2012	Ottawa Sand 20-30	1.279	108.19	6.02	1.20	8.19	1.64	9.32	1.86		291
6/22/2012	Ottawa Sand 20-30	1.079	108.35	5.65	1.13	7.59	1.52	10.10	2.02		292
6/25/2012	Ottawa Sand 20-30	1.074	107.81	7.05	1.41	8.48	1.70	10.00	2.00		293
4/30/2012	Angular Graded Sand	0.973	97.69	6.3	1.26	8.8	1.76	15.3	3.06	Movement @6.3, Sand boils	273
5/1/2012	Angular Graded Sand	0.968	97.20	6.2	1.24	10	2	14.7	2.94	Movement @ 6.3, Sand Boils	274
5/3/2012	Angular Graded Sand	0.983	98.66	6.3	1.26	9.1	1.82	14.4	2.88	Piping at 9.1 Spread and incre	299
5/10/2012	Angular Graded Sand	0.966	96.96	7.13	1.426			15.2	3.04	Piping in center, spreads to e	280
7/23/2012	Angular Graded Sand	0.943	94.70	8.70	1.74	11.50	2.3	15.50	3.1	Piping in middle	301
7/23/2012	Angular Graded Sand	0.946	95.01	7.02	1.404	11.10	2.22	14.60	2.92	Piping on side	302
7/25/2012	Angular Graded Sand	0.943	94.63	7.01	1.402	10.50	2.1	13.50	2.7	Piping in middle	303
7/26/2012	Angular Sand 20-30	0.909	91.21	7.50	1.50	7.50	1.50	12.75	2.55		305
7/27/2012	Angular Sand 20-30	0.913	91.68	7.50	1.50	9.70	1.94	14.60	2.92	0.25 - 0.5 high	306
7/30/2012	Angular Sand 20-30	0.936	93.97	7.20	1.44	9.00	1.80	13.40	2.68	0.5 - 1" high	307
8/1/2012	Garnet Sand	1.520	127.79	9.00	1.80	-		14.75	2.95	no pipe	309
8/1/2012	Garnet Sand	1.507	126.75	8.90	1.78	-		14.50	2.90	no pipe	310
8/2/2012	Garnet Sand	1.525	128.28	8.70	1.74	9.10	1.82	14.50	2.90	Sand boil in middle @9.1 incl	311
8/2/2012	Garnet Sand	1.544	129.85	8.00	1.60	8.50	1.70	14.00	2.80	Sand boil on side @8.5 inches	312

APPENDIX C

Summary of Constant Head Permeability Tests
CEE 6340 Spring 2011

	20/30 Ottawa Sand	Fine Ottawa Sand	Wasted Mortar Sand
Permeability*, k, cm/s	0.261	0.0491	0.0839
Coefficient of Uniformity, C_u	1.17	2.20	3.73
Void Ratio, e	0.523	0.510	0.576
Effective Particle Diameter, D_s, mm	0.668	0.320	0.359
$c_s \cdot c_L$	0.229	0.201	0.198

*Average of tests at $I = 1.0$

$$k = \frac{1}{36} c_s c_L \frac{\gamma_w}{\mu} D_S^2 \frac{e^3}{(1+e)}$$

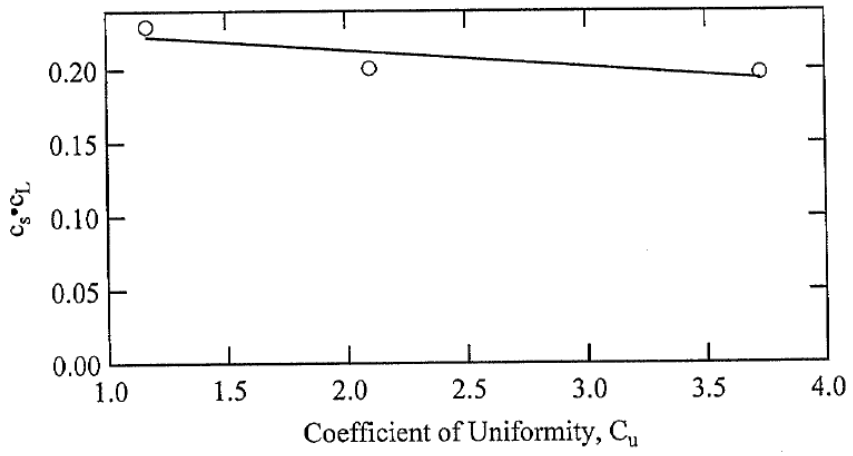

Fine Ottawa Sand

Mass Solids, m_s 712.85 g

Seive #	Initial mass seive (g)	Final mass seive (g)	Retained mass (g)	Cumulative mass retained m_i	%Finer	Portion of Sample Retained on Sieve, p	Average sphericity
20	483.20	483.50	0.3	0.3	99.96	4.21×10^{-4}	0.7
22	472.40	472.88	0.48	0.78	99.89	6.73×10^{-4}	0.7
25	475.39	478.02	2.63	3.41	99.52	3.69×10^{-3}	0.7
30	405.50	414.25	8.75	12.16	98.29	1.23×10^{-2}	0.8
40	351.18	706.77	355.59	367.75	48.41	0.499	0.85
50	432.94	609.55	176.61	544.36	23.64	0.248	0.9
60	431.87	494.81	62.94	607.30	14.81	8.83×10^{-2}	0.9
70	487.47	549.15	61.68	668.98	6.15	8.65×10^{-2}	0.9
80	406.80	428.83	22.03	691.01	3.06	3.09×10^{-2}	0.9
100	527.45	541.58	14.13	705.14	1.08	1.98×10^{-2}	0.9
120	404.20	409.72	5.52	710.66	0.31	7.74×10^{-3}	0.9
140	307.36	308.86	1.5	712.16	0.10	2.10×10^{-3}	0.9
Pan	397.92	398.26	0.34	712.5	0.05	4.77×10^{-4}	0.9
				0.05% loss			

$$\% \text{ Finer} = \left(1 - \frac{m_i}{m_s}\right) \times 100\%$$

D_{10} 0.227 D_{30} 0.333 D_{60} 0.476

C_U 2.10 C_C 1.03

Unified Soil Classification SP

Fine Ottawa Sand

Sieve 16	Proportion Retained, p*	D_{min} (mm) 1.18	D_{max}	D_{avg}	Average Sphericity, S	Specific Surface, SS	p×SS
20	4.21×10^{-4}	0.841	1.18	1.0105	0.7	8.4182	0.00357
22	6.73×10^{-4}	0.780	0.841	0.8105	0.7	10.576	0.00712
25	3.69×10^{-3}	0.701	0.780	0.7405	0.7	11.575	0.0427
30	1.23×10^{-2}	0.600	0.701	0.6505	0.8	11.530	0.1418
40	0.1199	0.425	0.600	0.5125	0.85	13.773	6.873
50	0.248	0.295	0.425	0.360	0.9	18.519	4.593
60	8.83×10^{-2}	0.250	0.295	0.2725	0.9	24.465	2.160
70	8.65×10^{-2}	0.210	0.250	0.230	0.9	28.986	2.507
80	3.09×10^{-2}	0.177	0.210	0.1935	0.9	34.453	1.065
100	1.98×10^{-2}	0.150	0.177	0.1635	0.9	40.775	0.8073
120	7.74×10^{-3}	0.125	0.150	0.1375	0.9	48.485	0.3753
140	2.10×10^{-3}	0.106	0.125	0.1155	0.9	57.720	0.1212
Pan	4.77×10^{-4}	0.075	0.106	0.0905	0.9	73.665	0.0351
						$\sum p\times SS = 18.732$	

$D_S =$ 0.3203 Ds corresponds with $D_?$ D_{29} $C_S \times C_L =$ _____

Equations $D_{avg} = \frac{D_{max} + D_{min}}{2}$ Specific Surface, $SS = \frac{6}{S \times D_{avg}}$ $D_S = \frac{6}{\sum(p_i \times SS_i)}$ $C_S \times C_L = 36\frac{k}{D_S^2}\frac{1+e}{e^3}\frac{\mu}{\gamma_w}$,

Coarse Ottawa Sand

Mass Solids, m_s 208.17

Seive #	Initial mass seive (g)	Final mass seive (g)	Retained mass (g)	Cumulative mass retained m_i	%Finer	Portion of Sample Retained on Sieve, p	Average sphericity
20	482.19	553.16	71.97	71.97	91.09	0.089	0.9
22	472.41	678.24	205.83	277.8	65.62	0.254	0.9
25	475.32	903.5	428.18	705.98	12.64	0.529	0.9
30	490.79	497.46	90.67	796.65	1.43	0.112	0.9
40	353.28	362.76	9.38	806.03	0.26	1.16×10^{-2}	0.9
50	431.26	435.23	0.87	806.9	0.26	1.07×10^{-2}	0.9
60	432.36	432.69	0.33	807.23	0.12	4.1×10^{-4}	0.9
70	487.76	488.18	0.42	807.65	0.06	5.2×10^{-4}	0.9
80	406.85	406.92	0.07	807.72	5.56×10^{-2}	8.7×10^{-5}	0.9
100	527.69	527.78	0.09	807.81	4.45×10^{-2}	1.11×10^{-4}	0.9
120	404.23	404.27	0.04	807.85	3.36×10^{-2}	9.95×10^{-5}	0.9
140	307.36	307.36	0.00	807.85	3.96×10^{-2}	0	0
Pan	397.95	398.00	0.05	807.9	3.3×10^{-2}	6.19×10^{-5}	0.9

$$\% \text{ Finer} = \left(1 - \frac{m_i}{m_s}\right) \times 100\%$$

D_{10} 0.681 D_{30} 0.754 D_{60} 0.796

C_U 1.169 C_C 1.049

Unified Soil Classification SP (Poorly graded sand)

Coarse Ottawa Sand

Sieve	Proportion Retained, p*	D_{min}	D_{max}	D_{avg}	Average Sphericity , S	Specific Surface, SS	p×SS
20	0.089	0.841	1.18	1.0105	0.9	6.597	0.5871
22	0.254	0.780	0.841	0.8105	0.9	8.225	2.089
25	0.529	0.701	0.780	0.7405	0.9	9.003	4.763
30	0.112	0.600	0.701	0.6505	0.9	10.249	1.148
40	1.16×10^{-2}	0.425	0.600	0.5125	0.9	13.008	0.1509
50	1.07×10^{-2}	0.295	0.425	0.360	0.9	18.519	0.1982
60	4.1×10^{-4}	0.250	0.295	0.2725	0.9	24.465	0.0100
70	5.2×10^{-4}	0.210	0.250	0.230	0.9	28.986	0.0151
80	8.7×10^{-5}	0.177	0.210	0.1935	0.9	34.453	0.0029
100	1.11×10^{-4}	0.150	0.177	0.1635	0.9	40.775	0.0045
120	4.45×10^{-5}	0.125	0.150	0.1375	0.9	48.485	0.0024
140	0	0.106	0.125	0.1155	0.9	57.720	0
Pan	6.19×10^{-5}	0.075	0.106	0.0905	0.9	73.665	0.0046

$\Sigma(p \times SS) = 8.9757$

$D_S =$ 0.668 Ds corresponds with $D_?$ D_8 $C_S \times C_L =$ 0.231

Equations $D_{avg} = \frac{D_{max} + D_{min}}{2}$ Specific Surface, $SS = \frac{6}{S \times D_{avg}}$ $D_S = \frac{6}{\Sigma(p_i \times SS_i)}$ $C_S \times C_L = 36 \frac{k}{D_S^2} \frac{1+e}{e^3} \frac{\mu}{\gamma_w}$,

Fine ottawa Sand
& Coarse Ottawa Sand

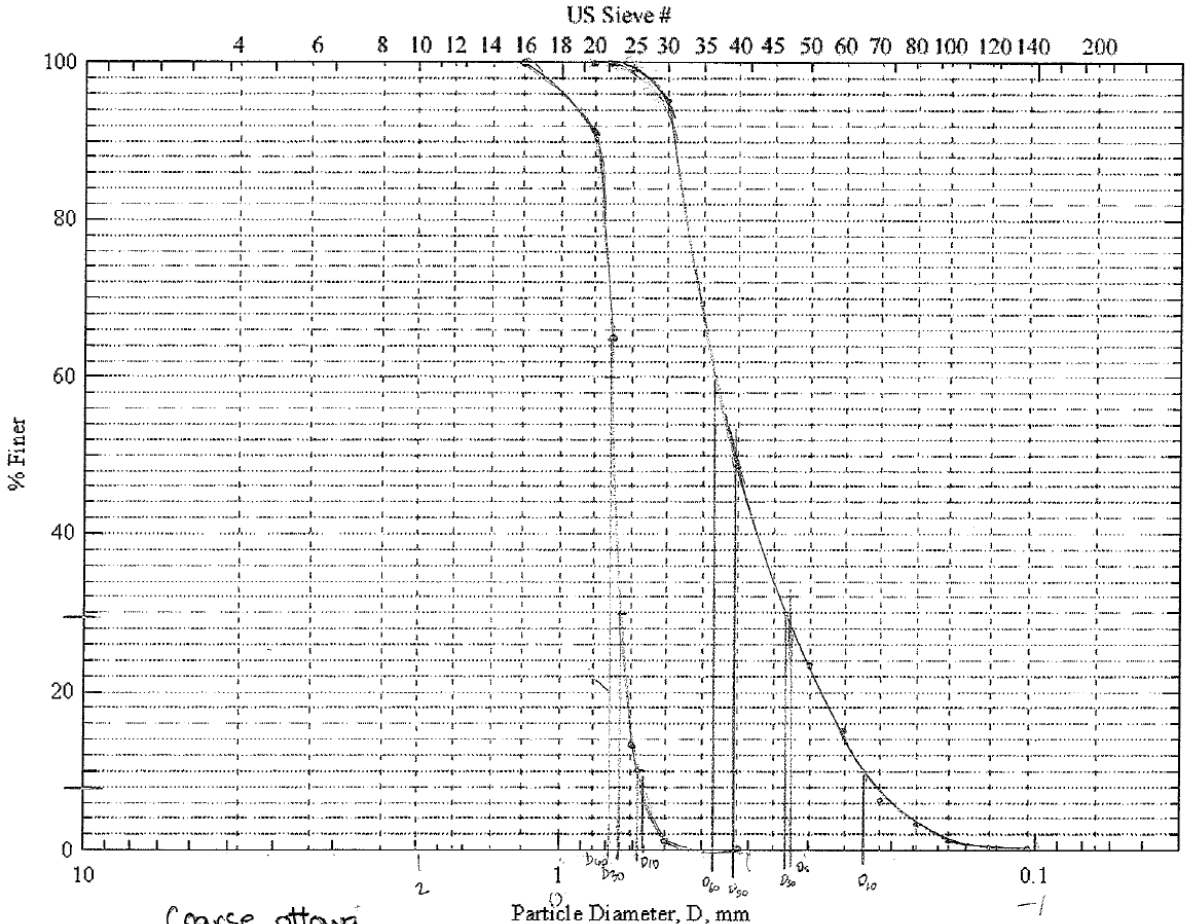

Coarse ottawa

D_{50} =
D_{60} = 0.796
D_{10} = 0.681
D_{30} = 0.754

Fine ottawa

D_{50} = 0.424 mm
D_{60} = 0.470 mm
D_{10} = 0.227 mm
D_{30} = 0.333 mm